AWARD NUMBER: W81XWH-13-1-0066

TITLE: Translational Control in Bone Marrow Failure

PRINCIPAL INVESTIGATOR: Marshall S. Horwitz

CONTRACTING ORGANIZATION: University of Washington
Seattle, WA 98195-9472

REPORT DATE: July 2016

TYPE OF REPORT: Final

PREPARED FOR: U.S. Army Medical Research and Materiel Command
Fort Detrick, Maryland 21702-5012

DISTRIBUTION STATEMENT: Approved for Public Release;
Distribution Unlimited

REPORT DOCUMENTATION PAGE

Form Approved
OMB No. 0704-0188

1. REPORT DATE	2. REPORT TYPE	3. DATES COVERED
July 2016	Final	1 May 2013 - 30 Apr 2016

4. TITLE AND SUBTITLE
Translational Control in Bone Marrow Failure

5a. CONTRACT NUMBER

5b. GRANT NUMBER
W81XWH-13-1-0066

5c. PROGRAM ELEMENT NUMBER

6. AUTHOR(S)
Marshall S. Horwitz

E-Mail: horwitz@uw.edu

5d. PROJECT NUMBER

5e. TASK NUMBER

5f. WORK UNIT NUMBER

7. PERFORMING ORGANIZATION NAME(S) AND ADDRESS(ES)

University of Washington
4333 Brooklyn Ave NE
Seattle, WA 98195-0001

8. PERFORMING ORGANIZATION REPORT NUMBER

9. SPONSORING / MONITORING AGENCY NAME(S) AND ADDRESS(ES)

U.S. Army Medical Research and Materiel Command
Fort Detrick, Maryland 21702-5012

10. SPONSOR/MONITOR'S ACRONYM(S)

11. SPONSOR/MONITOR'S REPORT NUMBER(S)

12. DISTRIBUTION / AVAILABILITY STATEMENT

Approved for Public Release; Distribution Unlimited

13. SUPPLEMENTARY NOTES

14. ABSTRACT
Severe congenital neutropenia (SCN) is an inherited bone marrow failure syndrome most often resulting from autosomal dominant or de novo transmission of heterozygous mutations in the gene, *ELANE*, encoding neutrophil elastase. Other causes of SCN include autosomal recessive inheritance of *HAX1* mutations. The purpose of this research is to understand how mutations in both *ELANE* and *HAX1* lead to neutropenia, in order to gain further understanding into normal homeostatic regulation of granulopoiesis and how it is disrupted in a variety of bone marrow failure syndromes. Based on identification of a new class of mutations in *ELANE* that disrupt the translational start site and recent findings that *HAX1* may be an RNA-binding protein, we originally hypothesized, and have now shown in patient-derived induced pluripotent stem cells (iPSC), that *ELANE* can encode amino-terminally truncated polypeptides initiating from internal translational start sites. In scope, we have proposed a series of experiments to be performed in cell culture systems to identify RNA sequences bound by HAX1, to determine if *ELANE* mutations influence HAX1 binding to *ELANE* mRNA and influence use of alternate translational start sites, and to biochemically characterize amino-terminally truncated neutrophil elastase. In the year since our last report, significant progress has been made in using new tools to model granulopoiesis, including generation of patient-derived iPSC and CRISPR-Cas9 genome-editing technology to introduce site specific repair or mutation into the *ELANE* locus, allowing for more relevant modeling of *ELANE* and HAX1 interactions in vitro.

15. SUBJECT TERMS
Neutropenia, bone marrow failure, neutrophil elastase, ELANE, HAX1, alternate translation, induced pluripotent stem cells (iPSC)

16. SECURITY CLASSIFICATION OF:			17. LIMITATION OF ABSTRACT	18. NUMBER OF PAGES	19a. NAME OF RESPONSIBLE PERSON
a. REPORT	b. ABSTRACT	c. THIS PAGE			USAMRMC
Unclassified	Unclassified	Unclassified	Unclassified	42	19b. TELEPHONE NUMBER *(include area code)*

Table of Contents

Page

N.b., per instructions referenced at http://mrmc.amedd.army.mil/index.cfm?pageid=researcher_resources.technical_reporting, awards issued prior to 1 October 2013 (such as this one) should be in the format of the specific award contract, which, although not linked from that page, can nevertheless be found here: http://mrmc.amedd.army.mil/index.cfm?pageid=researcher_resources.technical_reporting_pre_FY14
The two formats differ. In accord, with the instructions, we have therefore used the format described in the latter set of instructions.

1. INTRODUCTION

The overall goal of this project has been to determine how mutation of *ELANE*, encoding a neutrophil granule serine protease (neutrophil elastase), as well as a second gene, *HAX1*, produce inherited forms of neutropenia. We specifically focused on a recently described cluster of mutations occurring in the translational start site of ELANE, which would be predicted to disrupt expression of the protein and were incompatible with previous hypotheses relating to either mislocalization or misfolding of an expressed protein. We found that translational start site mutations force expression of neutrophil elastase from internal translation codons that bypass amino terminal processing steps required for appropriate localization and timing of zymogen activation. Over the course of this project, advances in iPSC generation and gene-editing technology have been adapted to study the pathogenesis of *ELANE*-related human neutropenia.

2. KEY WORDS

neutropenia
bone marrow failure
neutrophil elastase
ELANE
HAX1
alternate translation
induced pluripotent stem cells (iPSC)

3. OVERALL PROJECT SUMMARY

Current Objectives

The objective of the project is to determine how mutations in *ELANE* and/or *HAX1* produce neutropenia, toward the overall goal of obtaining a better understanding of the mechanisms of normal leukocyte homeostasis, identify final common pathways in different forms of hereditary neutropenia, and better understand how different types of mutations result in pathogenesis.

Results, Progress, and Accomplishments

Accomplishments are summarized in two resulting publications (Tidwell et al. 2014 *Blood* 123:562 & Nayak et al. 2015 *J Clin Invest* 125:3103) provided in the appendix and summarized as abstracts below.

Neutropenia-associated ELANE mutations disrupting translation initiation produce novel neutrophil elastase isoforms. (Tidwell et al. 2014 *Blood*) Hereditary neutropenia is usually caused by heterozygous germline mutations in the ELANE gene encoding neutrophil elastase (NE). How mutations cause disease remains uncertain, but two hypotheses have been proposed. In one, ELANE mutations lead to mislocalization of NE. In the other, ELANE mutations disturb protein folding, inducing an unfolded protein response in the endoplasmic reticulum (ER). In this study, we describe new types of mutations that disrupt the translational start site. At first glance, they should block translation and are incompatible with either the mislocalization or misfolding hypotheses, which require mutant protein for pathogenicity. We find that start-site mutations, instead, force translation from downstream in-frame initiation codons, yielding amino-terminally truncated isoforms lacking ER-localizing (pre) and zymogen-maintaining (pro) sequences, yet retain essential catalytic residues. Patient-derived induced pluripotent stem cells recapitulate hematopoietic and molecular phenotypes. Expression of the amino-terminally deleted isoforms in vitro reduces myeloid cell clonogenic capacity. We define an internal ribosome entry site (IRES) within ELANE and demonstrate that adjacent mutations modulate IRES activity, independently of protein-coding sequence alterations. Some ELANE mutations, therefore, appear to cause neutropenia via the production of amino-terminally deleted NE isoforms rather than by altering the coding sequence of the full-length protein.

Pathogenesis of ELANE-mutant severe neutropenia revealed by induced pluripotent stem cells. (Nayak et al. 2015 *J Clin Invest*) Severe congenital neutropenia (SCN) is often associated with inherited heterozygous point mutations in ELANE, which encodes neutrophil elastase (NE). However, a lack of appropriate models to recapitulate SCN has substantially hampered the understanding of the genetic etiology and pathobiology of this disease. To this end, we generated both normal and SCN patient–derived induced pluripotent stem cells (iPSCs), and performed genome editing and differentiation protocols that recapitulate the major features of granulopoiesis. Pathogenesis of ELANE point mutations was the result of promyelocyte death and differentiation arrest, and was associated with NE mislocalization and activation of the unfolded protein response/ER stress (UPR/ER stress). Similarly, high-dose G-CSF (or downstream signaling through AKT/BCL2) rescues the dysgranulopoietic defect in SCN patient–derived iPSCs through C/EBPβ-dependent emergency granulopoiesis. In contrast, sivelestat, an NE-specific small-molecule inhibitor, corrected dysgranulopoiesis by restoring normal intracellular NE localization in primary granules; ameliorating UPR/ER stress; increasing expression of CEBPA, but not CEBPB; and promoting

promyelocyte survival and differentiation. Together, these data suggest that SCN disease pathogenesis includes NE mislocalization, which in turn triggers dysfunctional survival signaling and UPR/ER stress. This paradigm has the potential to be clinically exploited to achieve therapeutic responses using lower doses of G-CSF combined with targeting to correct NE mislocalization.

Task 1. Perform "RIP-Seq" next-generation DNA sequencing of transcripts co-immunoprecipitating with HAX11

The goals of this task were to identify a consensus RNA sequence or structure for HAX1 binding, determine if there is a set of genes coordinately regulated at the post-transcriptional level by HAX1, and identify potential new candidate genes for genetically unexplained cases of neutropenia. In order to identify mRNAs bound by HAX1, we immunoprecipitated HAX1 from cell lysates and performed next-generation DNA sequence analysis of co-immunoprecipitating RNA species.

We developed a protocol for the co-immunoprecipitation of HAX1-bound mRNA and sequenced resulting products on the SOLiD platform. We obtained short fragments for several genes, as described in the year 1 progress report. As described in the Year 2 progress report, from the limited set of fragments recovered, it was not possible to derive a consensus primary or tertiary sequence. We evaluated approximately 20 probands from unexplained likely hereditary neutropenia cases, but did not identify potentially pathogenic variants in any of the genes showing possible HAX1 binding. Although we had planned to repeat these experiments in year 3, repeat immunoprecipitation proved unsuccessful, not producing RNA products suitable for sequencing, suggesting that HAX1 binding to mRNA may be artifactual

1a. Co-immunoprecipitate HAX1-mRNA complexes from HL60 cells (months 1-24).

The first year progress report describes successful completion of a RIP-Seq HAX1-mRNA co-immunoprecipitation protocol.

1b. Perform SOLiD sequencing of immunoprecipitated mRNA (months 1-6).

As previously noted in progress reports for years 1 and 2, we recovered fragments of the following genes: *EPHB2*, *ASTN1*, *CASP9*, and *FAF1*.

1c. Preliminary biocomputational analysis of sequence data, including mapping to reference genome (months 7-10).

Of the recovered genes, *EPHB2* was the most promising candidate, as it was enriched 16-fold in the immunoprecipitated fraction and because its expression is increased in neutropenic *Gfi-1*-deficient mice.

1d. Gene ontogeny and pathway characterization of identified mRNA species (months 11-13).

There were an insufficient number of genes to perform a gene ontogeny or similar pathway characterization.

1e. Consensus binding site determination (months 14-16).

No consensus binding site could be determined from the limited samples obtained upon sequencing.

1f. Troubleshoot sequencing failures, allow time for repetition and alternate approaches (months 17-24).

Unfortunately, the experiment was not reproducible, in that subsequent rounds of co-immunoprecipitation failed to yield significant recovery of co-precipitated mRNA compared to IgG controls. Overall, these experiments failed to confirm our hypothesis that HAX1 proteins binds *ELANE* or other mRNA sequences.

Task 2. Determine if *ELANE* mutations, particularly synonymous *ELANE* mutations, affect HAX1 binding and influence cryptic start site utilization.

Overall, we showed that several pathogenic *ELANE* mutations occurring at the translational start site or at sites of a predicted internal ribosome re-entry site (IRES) influence utilization of downstream ELANE ATG codons, resulting in amino-terminally truncated neutrophil elastase polypeptides that have the potential to bypass signal sequences directing subcellular routing and normal zymogen activation steps. We proposed that these "cryptic" polypeptides are therefore immediately catalytically active upon synthesis and are not properly contained within neutrophil granules and therefore have untoward effects on developing neutrophils. These results were published in Tidwell et al. *Blood* 2014;123:562-569 (appended). A proposed working model is shown in Fig. 6 of Tidwell et al. 2014.

2a. Prepare cDNA expression constructs for various mutations and express in RBL cells (months 1-36).

cDNA constructs for use in RBL expression assays were prepared as described in the Materials and Methods section of Tidwell et al. 2014.

2b. Prepare cDNA constructs for use in yeast 3-hybrid assay (months 1-6).

We prepared cDNA constructs for use in yeast 3-hybrid assays, as described in the progress report for year 1.

2c. Western blots to assay for internal start site utilization in transfected RBL cells (months 6-12).

Western blots confirm internal start site utilization in the presence of canonical *ELANE* translational start site mutations (Fig. 2 of Tidwell et al. 2014) and pathogenic mutations occurring in predicted IRES sequences (Fig. S3 of Tidwell et al. 2014) in transfected RBL cells as well as for canonical translation start site mutations in patient-derived iPSC subject to granulopoietic differentiation conditions (Fig. S3 of Tidwell et al. 2014).

2d. Prepare vectors containing mutations for IRES test assay (months 3-9).

Vectors for IRES test assay were prepared as described in the Materials and Methods section of Tidwell et al. 2014.

2e. Develop IRES test assay in HeLa cells (months 9-12).

We developed an IRES test assay system and showed that neutropenic mutations contained within the predicted IRES or nearby disrupted translation initiating from internal ATG codons using a combination of Luciferase assays (Fig. 3 of Tidwell et al. 2014) and confirmatory western blots (Fig. S4 of Tidwell et al. 2014).

2f. Perform yeast 3-hybrid assays with mutant constructs (months 15-36).

Yeast 3-hybrid assays failed to reproducibly demonstrate interactions between *ELANE* mRNA and HAX1 protein. Taken together with the co-immunoprecipitation experiments which similarly failed to recover *ELANE* mRNA fragment, we now question whether HAX1 protein directly associates with *ELANE* mRNA. The experimental hypothesis concerning how some *ELANE* mutations may affect translation of *ELANE* mRNA, as we

originally proposed, via disruption of interactions with the ribosome at sites of canonical translation initiation or IRES sequences appears largely supported by our experimental findings. However, we were unsuccessful in our endeavors to show that *HAX1* mutations function through a unified mechanism and we consider that portion of our original hypothesis to be largely unsupported by the subsequent experiments we performed here.

2g. Develop HAX1 RNAi assay in HL60 cells (months 20-36).

An initial attempt to deplete HAX1 RNA using RNA interference in HL60 cells was unsuccessful. Given a lack of supporting results from Tasks 1 and 2f, and unexpected advanced in iPSC and genome-editing technology that resulted in a revised SOW with new experiments to perform, we deprioritized this task as we felt it would not contribute significantly to progress toward overall understanding of the pathogenesis of *ELANE* and *HAX1*-mediated hereditary neutropenia.

2h. Employ in vitro differentiation of patient-derived iPSC models to determine how *ELANE* mutations influence cryptic start site utilization (months 18-36).

We were successful in repeating experiments performed in cell lines in patient-derived iPSC gene models, including using CRISPR genome editing, as overall described in Tidwell et al. 2014 and Nayak et al. 2015.

Task 3. Characterize the biochemical properties of internally-translated neutrophil elastase polypeptides (months 14-36).

In summary, as shown in the Tidwell et al. 2014 and Nayak et al. 2016 publications, the internally-translated neutrophil elastase polypeptides retain catalytic activity, mislocalize, do not show evidence of induction of the unfolded protein response, reduce clonogenic growth, have no significant effect on apoptosis in transfected RBL cells but do show a slight increase of apoptosis in patient-derived iPSC, and when expressed in iPSC demonstrate reduced production of neutrophils.

3a. Prepare cDNA expression constructs for each of the internally translated polypeptides for transfection into RBL cells (months 14-17).

cDNA constructs incorporating pathogenic ELANE mutations at the translational start site and predicted IRES, as well as internal controls, were constructed as described in the Materials and Methods sections of Tidwell et al. 2014 and Nayak et al. 2015.

3b. Determine if internally translated polypeptides are catalytically active when transfected into RBL cells (months 18-24).

We found that residual catalytic activity is retained by internally translated neutrophil elastase polypeptides commencing from constructs with observed mutations in the canonical *ELANE* translational start site (Figs. 5A and S6 of Tidwell et al. 2014). For more conventional missense substitutions, we showed that proteolytic inhibition with the small molecule specific inhibitor of neutrophil elastase, sivelestat, can restore iPSC differentiation capacity (Fig. 6 of Nayak et al. 2015).

3c. Determine the subcellular localization of internally translated polypeptides by immunofluorescent staining within transfected RBL cells (months 24-26).

We found that internally translated neutrophil elastase polypeptides aberrantly sublocalized to the nucleus of transfected RBL cells (Fig. S10 of Tidwell et al. 2014).

3d. Determine subcellular localization of internally translated polypeptides based on subcellular fractionation (months 27-29).

We attempted but technically failed to satisfactorily complete subcellular fractionation experiments and therefore have no data to report for this sub-task.

3e. Determine if internally translated polypeptides induce expression of ER or other cellular stress markers (months 30-33).

We did not find induction of ER stress as measured by HSPA5 expression (Figs. 5B and S7 of Tidwell et al. 2014).

3f. Evaluate for apoptotic effects of transfected internally translated polypeptides (months 33-36).

With respect to apoptosis, in transfected RBL cells, there was no evidence of increased apoptosis as measured by annexin V staining (Figs. 5C and S8 of Tidwell et al. 2014) or qRT-PCR of a set of genes induced with apoptosis (Fig. S9 of Tidwell et al. 2014). Results were somewhat different when evaluating the same mutations in patient-derived iPSC models, where a small but definite increase in apoptotic cells as detectable using FACS analysis of annexin V staining under granulocytic differentiation conditions (Fig. S3B of Tidwell et al. 2014). These results expose inadequacies in the use of cultured cell models and demonstrate the superiority of iPSC as models of understanding hereditary neutropenia resulting from *ELANE* mutations.

3g. Develop a flow-sorting based clonogenic assay to evaluate for toxic effects on cell growth of internally translated polypeptides upon transfection of U937 cells (months 33-36).

We developed a clonogenic growth assay employing single cell sorting, as described in the Materials and Methods section of Tidwell et al. 2014. U937 cells transfected with *ELANE* expression constructs reproducing patient-derived translational start site mutations demonstrate reduced clonogenic capacity (Fig. 4 of Tidwell et al. 2014), which serves as a proxy for neutropenia in this cellular model system.

3h. Use patient-derived iPSC models and CRISPR/Cas9 genome-editing to generate a range of ELANE mutations and determine how they alter biochemical properties of neutrophil elastase as well as alter in vitro hematopoietic differentiation (months 21-36).

This added task was largely addressed in the Nayak et al. 2015 publication. At least for conventional amino acid missense substitutions of ELANE, gene correction can reverse granulocytic differentiation defects and neutrophil elastase mislocalization. Another significant finding was the protease inhibition with a small molecule inhibitor, sivelestat, can similarly restoring granulopoiesis, suggesting a potential new avenue for therapy.

Discussion

Our studies have informed understanding of hereditary forms of neutropenia and other bone marrow failure syndromes, including myelodysplasia (which is a complication of hereditary neutropenia) by addressing how the most abundant protein of leukocytes, neutrophil elastase, contributes to the normal homeostatic regulation of blood cells. We have developed new patient-derived iPSC models of myelopoiesis and have validated that they faithfully recapitulate molecular genetic and cellular features occurring in the bone marrow, thus extending their use for analysis of other forms of hereditary blood disorders.

Beyond the scope of this proposal, and still in the future, gene-correction of *ELANE* mutations, as demonstrated here using CRISPR-Cas9 technology, may ultimately prove

to be of use as a therapeutic tool for treating congenital neutropenia and other hereditary blood disorders.

Additionally, acquired forms of neutropenia, such as from chemotherapy, autoimmune disorders, or premalignant conditions, are not uncommon and likely involve common denominators that molecular studies of congenital disorders may help to reveal.

4. KEY RESEARCH ACCOMPLISHMENTS

- Identification of alternate translation start sites in ELANE.
- Formal validation that ELANE mutations are sufficient for disease causality utilizing genome editing technologies.
- Confirmation of mislocalization and unfolded protein-induced stress in iPSC models of human disease.
- Indication that protease inhibition can reverse pathogenic features in model systems of the disease, thereby pointing the way toward novel therapy.
- Still unresolved is the role of HAX1 in contributing to disruption of neutrophil elastase.

5. CONCLUSION

In general, our studies have illuminated unconventional ways through which primary coding sequence mutations in genes may have unexpected effects on translation, including by disrupting translational start sites, activating internal ribosome entry sites, or affecting mRNA folding and interactions with RNA binding proteins. Given the large volume of ‘variants of undetermined significance’ now pouring in from whole genome and whole exome sequencing studies, our results may have bearing on the interpretation of rare variants that either do not directly alter protein coding or that are otherwise predicted to have benign effects on protein structure and function.

These experiments helped to pave the way for an extension of this project in the form a new NIH R01 project (NIH R01 130472, Pathogenesis of ELANE-related neutropenia).

6. PUBLICATIONS, ABSTRACTS, AND PRESENTATIONS

a. Manuscripts

Tidwell, T., Wechsler, J., Nayak, R.C., Trump, L., Salipante, S.J., Cheng J.C., Donadieu, J., Glaubach, T., Corey, S.J., Grimes, H.L., Lutzko, C., Cancelas, J.A., and Horwitz, M.S. (2014) Neutropenia-associated *ELANE* mutations disrupting translation initiation produce novel neutrophil elastase isoforms. **Blood** 123:562-569.

Nayak, R., Trump, L., Aronow, B.J., Myers, K., Mehta, P., Kalfa, T., Wellendorf, A.M., Horwitz, M.S., Grimes, H.L., Lutzko, C., and Cancelas, J.A. Pathogenesis of ELANE-mutant severe congenital neutropenia revealed by patient-derived induced pluripotent stem cells. **J Clin Invest** 125:3103-3116.

b. Presentations made during the last year

None

7. INVENTIONS, PATENTS AND LICENSES

None

8. REPORTABLE COUTCOMES

- Creation of iPSC as models of human hereditary neutropenia.
- Generation of CRISPR-Cas9 *ELANE* gene correction tools.

9. OTHER ACHIEVEMENTS

Supported personnel did benefit from career development as a result of their participation in technological aspects of the project.

Donovan Anderson, further developed bioinformatic skills by participating in seminars and classes involving the R programming language, Bioconductor, and next generation DNA/RNA sequence analysis.

Timothy Tidwell, a graduate student obtained his Ph.D. for work based on pursuit of this project (though he was supported largely through other means, including an NIH T32 training grant). Dr. Tidwell has recently moved to a postdoctoral position at the University of Utah.

10. References

None additional cited

11. APPENDICES

Publications attached.

Regular Article

PHAGOCYTES, GRANULOCYTES, AND MYELOPOIESIS

Neutropenia-associated *ELANE* mutations disrupting translation initiation produce novel neutrophil elastase isoforms

Timothy Tidwell,[1] Jeremy Wechsler,[1] Ramesh C. Nayak,[2] Lisa Trump,[2] Stephen J. Salipante,[3] Jerry C. Cheng,[4] Jean Donadieu,[5] Taly Glaubach,[6] Seth J. Corey,[6] H. Leighton Grimes,[2,7] Carolyn Lutzko,[2,8,9] Jose A. Cancelas,[2,10] and Marshall S. Horwitz[1]

[1]Department of Pathology, University of Washington School of Medicine, Seattle, WA; [2]Division of Experimental Hematology and Cancer Biology, Cincinnati Children's Hospital Medical Center, Cincinnati, OH; [3]Departments of Laboratory Medicine and Genome Sciences, University of Washington School of Medicine, Seattle, WA; [4]Kaiser Permanente, Los Angeles Medical Center and David Geffen School of Medicine at UCLA, Los Angeles, CA; [5]French Severe Chronic Neutropenia Registry, Hospital Trousseau, Paris, France; [6]Department of Pediatrics, Northwestern University Feinberg School of Medicine, Chicago, IL; [7]Division of Immunobiology, Cincinnati Children's Hospital Medical Center, Cincinnati, OH; [8]Division of Regenerative Medicine and Cellular Therapies, Hoxworth Blood Center, University of Cincinnati College of Medicine, Cincinnati, OH; [9]Translational Core Laboratories, Division of Experimental Hematology and Cancer Biology, Cincinnati Children's Hospital Medical Center, Cincinnati, OH; and [10]Research Division, Hoxworth Blood Center, University of Cincinnati College of Medicine, Cincinnati, OH

Key Points

- *ELANE* mutations in the first codon and Kozak sequence yield amino-terminally truncated NE lacking pre and pro sequences.
- The study implies that sometimes NE coding sequence changes are incidental and noncoding *ELANE* variants are pathogenic.

Hereditary neutropenia is usually caused by heterozygous germline mutations in the *ELANE* gene encoding neutrophil elastase (NE). How mutations cause disease remains uncertain, but two hypotheses have been proposed. In one, *ELANE* mutations lead to mislocalization of NE. In the other, *ELANE* mutations disturb protein folding, inducing an unfolded protein response in the endoplasmic reticulum (ER). In this study, we describe new types of mutations that disrupt the translational start site. At first glance, they should block translation and are incompatible with either the mislocalization or misfolding hypotheses, which require mutant protein for pathogenicity. We find that start-site mutations, instead, force translation from downstream in-frame initiation codons, yielding amino-terminally truncated isoforms lacking ER-localizing (pre) and zymogen-maintaining (pro) sequences, yet retain essential catalytic residues. Patient-derived induced pluripotent stem cells recapitulate hematopoietic and molecular phenotypes. Expression of the amino-terminally deleted isoforms in vitro reduces myeloid cell clonogenic capacity. We define an internal ribosome entry site (IRES) within *ELANE* and demonstrate that adjacent mutations modulate IRES activity, independently of protein-coding sequence alterations. Some *ELANE* mutations, therefore, appear to cause neutropenia via the production of amino-terminally deleted NE isoforms rather than by altering the coding sequence of the full-length protein. (*Blood*. 2014;123(4):562-569)

Introduction

There are two main types of hereditary neutropenia: cyclic neutropenia and severe congenital neutropenia (SCN). In cyclic neutropenia, neutrophil counts oscillate with 21-day periodicity.[1] In SCN, neutrophil counts are statically low, promyelocytic maturation arrest occurs in the bone marrow, and disease often progresses to myelodysplasia or acute myeloid leukemia.[1] Heterozygous mutation of *ELANE* causes almost all cases of cyclic neutropenia[2] and the majority of SCN.[3] Because neutropenia is often lethal, germline mutations frequently arise de novo.[1] Additional genes causing SCN include *HAX1*,[4] *GFI1*,[5] *G6PC3*,[6] and others.[7]

ELANE encodes the neutrophil granule serine protease, neutrophil elastase (NE).[8] While it is unclear how *ELANE* mutations cause neutropenia, nearly all of its myriad mutations are either amino acid missense substitutions, small insertions or deletions preserving translational reading frame, or carboxyl-terminal chain-terminating mutations escaping nonsense-mediated decay.[1,9] The mutational spectrum would seem to exclude haploinsufficiency as a mechanism, because mutations predicting an absence of protein have not yet been reported.

Mutations distribute throughout NE, and effects on biochemical properties such as proteolytic activity, serpin inhibition, and glycosylation appear inconsistent.[9-11] Two theories on how mutations affects NE have been proposed. In one, mutant NE is mistrafficked, while, in the other, mutant NE misfolds, activating an unfolded protein response (UPR) in the endoplasmic reticulum (ER).

Relevant to the mistrafficking hypothesis, NE is stored in lysosome-like granules, but distributes to the plasma membrane

Submitted July 4, 2013; accepted October 28, 2013. Prepublished online as *Blood* First Edition paper, November 1, 2013; DOI 10.1182/blood-2013-07-513242.

Presented in abstract form at the 2012 annual meeting and exposition of the American Society of Hematology, Atlanta, GA, December 8, 2012.

The online version of this article contains a data supplement.

There is an Inside *Blood* commentary on this article in this issue.

The publication costs of this article were defrayed in part by page charge payment. Therefore, and solely to indicate this fact, this article is hereby marked "advertisement" in accordance with 18 USC section 1734.

and nucleus.[8] Some *ELANE* mutations are reported to disturb NE trafficking, both in vitro[12,13] and in vivo[10] (though other studies have not found mislocalization).[9] Furthermore, mutations in the gene encoding the lysosomal transporter protein AP3B1, which is involved in trafficking NE,[12] are responsible for the neutropenic disorders Hermansky-Pudlak syndrome type 2[14] and canine cyclic neutropenia,[12] and, at least in dogs, NE appears to be mislocalized.[15] Chédiak-Higashi syndrome, caused by mutations in a different lysosomal trafficking protein, may also cause neutropenia,[16] and in a mouse model of the disorder, NE appears to be mistrafficked.[17] Finally, mutations in other genes involved in lysosomal trafficking, including *VPS13B*[18] and *VPS45*,[19,20] also cause neutropenia.

With the misfolding hypothesis, when certain *ELANE* mutations are expressed in vitro, UPR markers including binding immunoglobulin protein, XBP1, and GRP78 are upregulated.[10,21] A supportive observation involves Wolcott-Rallison syndrome, which, in addition to other features, includes neutropenia and is caused by mutations in protein kinase RNA-like ER kinase (PERK) which functions as a sensor of ER stress.[22] Gene-targeted mice carrying a neutropenia-associated *ELANE* mutation develop neutropenia when ER degradation is blocked with the proteasome inhibitor bortezomib, resulting in high levels of ER stress.[23]

Here, we describe a new category of *ELANE* mutation disrupting the translation initiation codon or the immediately adjacent Kozak sequence that does not easily fit with either the mislocalization or misfolding hypotheses. Because they might not produce a protein, these mutations would seem contrary to the concept that a mutant polypeptide causes disease. The aim of the present study is to determine the molecular effects of mutations involving *ELANE*'s initiation codon.

Materials and methods

Mutational analysis

Sanger DNA sequencing of *ELANE* from polymerase chain reaction (PCR)-amplified peripheral blood genomic DNA was performed as described.[2] Research was approved by the University of Washington Institutional Review Board, and participants gave written informed consent in accordance with the Declaration of Helsinki.

Induced pluripotent stem cell (iPSC) generation

Peripheral blood mononuclear cells were transduced using lentiviral vectors containing *Oct4*, *Sox2*, *Klf4*, and *c-Myc*. See details in supplemental Materials and methods section on the *Blood* Web site.

Cell culture

Human leukemic monocyte lymphoma (U937) and human promyelocytic leukemia (HL-60) cell lines were purchased from ATCC and cultured in RPMI 1610 (Life Technologies, Grand Island, NY). Henrietta Lacks (HeLa) and rat basophil leukemia 1 (RBL-1) cells were cultured in Dulbecco's modified eagle medium (Life Technologies). Media was supplemented with 10% fetal bovine serum containing 100 units/mL penicillin and 100 μg/mL streptomycin.

IRES experiments

ELANE segments were PCR-amplified from genomic DNA and inserted into a bicistronic (pRF) vector (gift from Dr. Vincent Mauro, The Scripps Research Institute, La Jolla, CA), containing firefly and *Renilla* luciferase. A construct containing the triplicated active region was made by separating 3 tandem repeats with a 9-bp oligonucleotide derived from a non–internal ribosome entry site (IRES) region from the mouse β-globin gene[24] (supplemental Table 1). Vectors were transfected into HeLa cells using Fugene HD (Promega, Madison,WI). Cells were harvested after 24 hours. Luciferase assays were performed using the Dual-Luciferase Reporter Assay System (Promega) on a Synergy 4 microplate reader (BioTek, Winooski, VT). Firefly activity was normalized to *Renilla* activity.

Western blotting

Chicken IgY raised against the NE carboxyl-terminus was used for western blots, as described.[25]

Clonogenic capacity assay

Wild-type and mutant *ELANE* vectors were generated by inserting *ELANE* into pIRES2-ZsGreen (Clonetech, Mountain View, CA) obtained from previously described vectors.[11] U937 cells were transfected with the Amaxa Nucleofector Kit C (Lonza, Basel, Switzerland), 2 μg of DNA, and program W-01. After 24 hours posttransfection, single cells were sorted into 96 well plates using a FACSAria II (BD Biosciences, San Jose, CA), gated on ZsGreen fluorescent protein expression. Two weeks later, plates were scored for wells containing ≥ 20 cells.

ER stress and apoptosis assay

HL-60 cells were transfected with the same vectors as the clonogenic capacity assay, with 1.25% dimethylsulfoxide.[26] ZsGreen-positive cells were sorted with a FACSAria II, and RNA was isolated using RNeasy Plus Mini Kits (Qiagen, Germantown, MD). RNA was reverse-transcribed with SuperScript II reverse transcriptase (Life Technologies). Heat-shock 70-kDa protein 5 (*HSPA5*) (Hs00607129_gH) expression, normalized to *ACTB* (4352935E) was quantified using TaqMan (Life Technologies) assays on an Applied Biosystems 7300 real-time PCR instrument. ER stress was induced in control cells with 2 μg/mL tunicamycin for 16 hours. For apoptosis assays, transfected HL-60 cells were incubated for 24 hours, and then serum-starved for 16 hours. Apoptosis was assessed with the Annexin V-PE Apoptosis Detection Kit 1 (BD Pharmingen) per manufacturer instructions on a FACSCanto II, gating ZsGreen-positive cells.

Proteolytic activity assay

Proteolytic activity was assessed as described,[11] following 16-hour incubation.

Statistical methods

Comparisons between groups employed Student two-tailed *t* test.

Results

Mutations disrupting the *ELANE* translational start site

An SCN-associated *ELANE* mutation, with A>G substitution at the first position of the ATG methionine translation initiation codon (Table 1), was reported previously by the French Neutropenia Register.[27] Neither parent was affected or possessed the mutation, indicating it arose de novo. As an isolated case, it remained uncertain whether the mutation was causative. Since then, the proband has had an affected child inheriting the mutation, and we have observed another de novo occurrence in an unrelated patient in the French Register. The same mutation, again de novo, has subsequently been described in two additional, unrelated patients,[9,28] including one unresponsive to recombinant human granulocyte colony stimulating factor therapy.[28] Recently, additional SCN patients with mutations of the second (T>G) and third (G>C) positions of the ATG methionine initiation codon have been described,[9] and, in the case of the former, was also seen in the French Register (Table 1).

Table 1. *ELANE* translational start-site mutations

cDNA (NM_001972.2)	No. of probands	Phenotype	Kozak Sequence						References
			a	c	c	A	T	G	
c.-3A>T	1	Cyclic neutropenia	t						This report
c.1A>G	4	SCN				g			9, 27, 28; This report
c.2T>G	2	SCN					g		9; This report
c.3G>C	1	SCN						c	9
c.3G>A	1	SCN						a	This report

We report here for the first time, a different mutation (G>A) at the third position of the ATG initiation codon arising de novo in an SCN patient, whose affected child also inherited the mutation (Table 1 and supplemental Figure 1A). Also for the first time, we describe a cyclic neutropenia patient with mutation (A>T) of the conserved −3 position of the Kozak translation initiation sequence, where a purine, as found in wild-type *ELANE*, is strongly preferred[29] (Table 1 and supplemental Figure 1B).

In summary, there were 9 unrelated probands with neutropenia comprising 5 different translation start mutations (Table 1). No other *ELANE*-coding sequence variants were observed among these patients. These variants have not been described in 6503 individuals in the National Heart, Lung, and Blood Institute's Exome Sequencing Project (http://evs.gs.washington.edu), cataloged in 1000 Genomes,[30] dbSNP[31] (version 135), or among hundreds of controls.[9] Since these variants were exclusively found in patients with neutropenia who lacked other causative mutations, and often arose de novo, but can be autosomally dominantly transmitted, we conclude that they are causal. Among a total of 191 different known *ELANE* mutations,[9] all, except for these, were predicted to result in translation of correspondingly mutated NE protein. A closer look at this class of mutations is warranted.

ELANE start-site mutations activate translation from downstream initiation codons

We hypothesized that instead of preventing translation of NE, mutations of *ELANE*'s translational start site may, instead, lead to translation commencing from internal methionine ATG codons. There are three downstream, in-frame ATG codons that could potentially be used as start sites when the canonical initiation codon is mutated (Figure 1A). (There are also two out-of-frame initiation codons. One is followed immediately afterward by a stop codon, and the other is terminated after 9 codons.)

To test this possibility, we transfected *ELANE* complementary DNA (cDNA) containing mutations involving the initiation codon and the Kozak sequence in RBL-1 cells (which are conventionally employed for the study of NE because although they lack endogenous NE, they correctly target it to granules),[32] and performed a western blot with an antibody detecting a carboxyl-terminal epitope. When the initiation codon was mutated from ATG to either ATA or GTG, shortened forms of NE were evident (Figure 2, c.3G>A, c.1A>G). When the highly conserved nucleotide in the Kozak sequence 3 nucleotides upstream from the initiation codon was mutated from A to T, shorter proteins were produced along with the wild-type protein (Figure 2, c.-3A>T). To verify that shortened forms of NE represent translation initiation from alternate sites and are not due to post-translational processing, expression vectors were generated containing just the open reading frames (ORFs) representing all in-frame methionine codons (wild-type compared with ATG2, ATG3, and ATG4). Correspondingly shorter isoforms were also produced when the region upstream from each internal in-frame ATG was deleted, with the exception that there was no detectable expression from ATG4 ORF (Figure 2).

We tested for the presence of shorter NE isoforms in patient-derived samples. Bone marrow was unavailable in patients with start-site mutations. Western blot performed on peripheral blood could not be interpreted due to neutropenia (not shown). We, therefore, generated iPSC from a patient with the c.1A>G mutation (supplemental Figure 2), which showed normal karyotype, pluripotent stem-cell marker expression, and the ability to differentiate into all three germ layers. Compared with control, upon hematopoietic differentiation, there was no significant difference in the level of $CD34^+$ cells, but subsequent myeloid differentiation demonstrated the following: fewer bands and neutrophils; increased promyelocytes, myelocytes, and metamyelocytes; more monocytes; and increased apoptosis of $CD34^-/CD33^+$ cells (supplemental Figure 3A-D). (The extent of apoptosis, however, may fall short of explaining cytopenias and could be an epiphenomenon.) Western blot of $CD34^-/CD13^+/CD11b^{low}/CD15^{++}$ myeloid cells derived from iPSC (supplemental Figure 3E) confirmed reduced abundance of full-length NE (as expected with heterozygosity for the mutation, where wild-type is also present) and uniquely increased abundance of at least one shorter isoform. Additional higher molecular weight products, as seen in RBL-1 cells, were detected. Isoform sizes in iPSC appeared to be slightly shifted upward, compared with RBL-1 cells, suggesting differences in posttranslational modification. Experiments with iPSC, therefore, corroborate phenotype and downstream initiation of translation.

Defining an *ELANE* IRES

Figure 2 shows that translation normally initiating from the canonical ATG1 start site in wild-type *ELANE* does not lead to translation of polypeptides from internal ORFs. However, the ATG2 ORF expression vector yields a range of shorter polypeptides corresponding to translation initiation from ATG2, ATG3, and ATG4. We reasoned

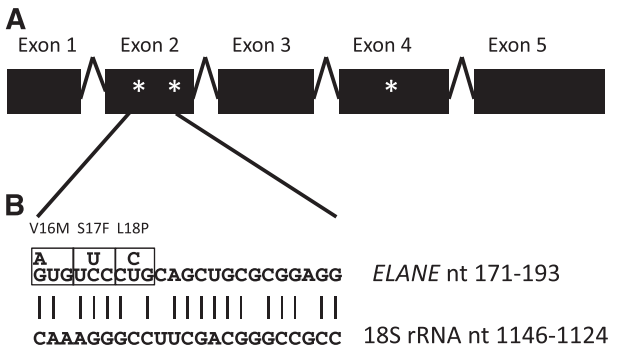

Figure 1. Location of downstream in-frame ATG codons in *ELANE* mRNA and IRES structure. (A) Schematic of *ELANE* mRNA. In-frame downstream ATG codons that may be used as initiation start sites (asterisks). (B) Potential *ELANE* IRES showing complementarity to 18S rRNA. Nucleotide substitutions introduced by p.V16M, p.S17F, and p.L18P mutations are marked.

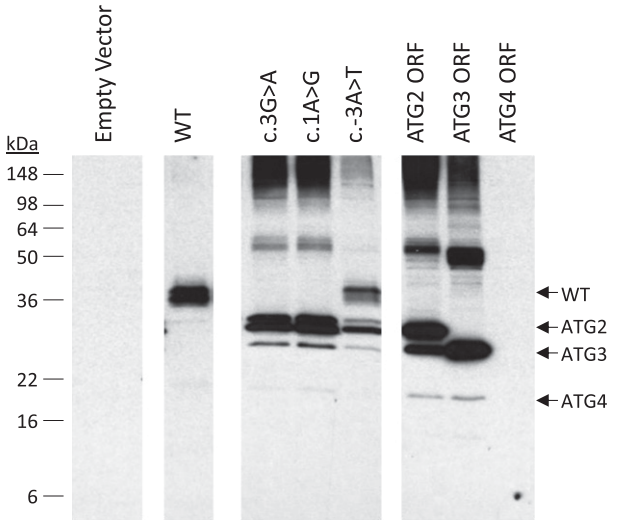

Figure 2. Western blot of RBL-1 cells transfected with *ELANE* vectors containing translational start-site mutations, using an antibody to the carboxyl terminus of NE. Mutations of the canonical methionine initiation codon (c.3G>A and c.1A>G) and the noncoding Kozak sequence (c.-3A>T) lead to expression of shorter isoforms of *ELANE*. When the upstream region is removed and only the ORF that corresponds to each ATG codon is expressed, separated isoforms are identifiable (ATG2 ORF, ATG3 ORF, and ATG 4 ORF). Molecular weight markers (in kDa; right) and NE isoforms (arrows; left) are shown.

that there could be an IRES situated between ATG2 and ATG3. IRES sequences are regions of messenger RNA (mRNA) that recruit the ribosome to sites adjacent to internal ATG codons and permit internal initiation of translation in a cap-independent manner.[33]

To confirm the presence of an IRES and exclude the possibility that the cap site is still used for ribosome entry when the canonical initiation codon is mutated, we introduced a termination codon (c.83C>A = p.S-2X) between ATG1 and the first internal methionine codon, ATG2, in *cis* with the Kozak sequence mutation (c.-3A>T). The shorter isoforms were present in greater abundance, while polypeptides initiating from ATG1 terminated prior to the carboxyl terminus and were consequently no longer detected by antibody to the carboxyl-terminus (supplemental Figure 4).

One IRES, found in mouse *Nkx6-2*, exhibits reverse complementarity to 18S ribosomal RNA (rRNA), and mutations disturbing complementarity between *Nkx6-2* mRNA and 18S rRNA disrupt IRES activity.[34] We scrutinized *ELANE* mRNA and confirmed it contains a region of reverse complementarity to 18S rRNA just downstream from ATG2, spanning the region of complementarity to 18S rRNA defined in *Nkx6-2* (Figure 1B). In computer simulations where random sequences the same length as the putative IRES were generated from *ELANE* mRNA and compared with 18S rRNA, sequence complementarity was determined to be highly non-random ($P = 1.3 \times 10^6$) (supplemental Figure 5).

We, therefore, evaluated whether the region of 18S rRNA complementarity possesses IRES activity. A test vector containing distinguishable tandem luciferase (*Renilla* and firefly) reporters, was used. The potential IRES was inserted in-between the two luciferase genes. The upstream *Renilla* luciferase contains a Kozak consensus sequence needed for translation initiation; however, translation of the downstream firefly luciferase requires that the inserted sequences possess IRES activity. Several overlapping segments from within the region of *ELANE* exhibiting complementarity to 18S rRNA for IRES activity in transfected HeLa cells were tested. Region 1 showed a 2.5-fold increase in IRES activity, but regions 2 and 3 did not exhibit IRES activity compared with vector alone (Figure 3A), possibly due to the presence of additional start codons within those regions. Additionally, a 5′-UTR of similar length from an arbitrary gene (*KLHDC8B*) lacked IRES activity (not shown). To further verify that region 1 contained an IRES, we evaluated its activity when it was triplicated in a head-to-tail sequence. IRES activity was increased by ~sixfold, compared with the vector alone (Figure 3B), suggesting that IRES activity is not adventitious.

ELANE mutations activating the IRES

It should be noted that *ELANE* mutations frequently locate to the putative IRES.[1,9] We tested 3 of these mutations (p.V16M, p.S17F, and p.L18P) for effect upon IRES activity, using the dual luciferase reporter containing triplicated *ELANE* IRES (Figure 3B). Two of the mutations (p.V16M and p.S17F) markedly increased activity, compared with the empty vector. When transfected into RBL-1 cells (supplemental Figure 4), p.V16M produced one of the shorter isoforms also seen with the c.-3A>T mutation. Results for S17F were inconclusive because there was limited expression of even the wild-type isoform, which would also be consistent with the possibility that S17F disrupts translation from the canonical start site. Further study is needed to determine the nature of polypeptides produced by these mutations, optimal sequence for IRES function, and how mutations within *ELANE* mRNA may modulate IRES activity.

Effect of amino-terminally truncated NE on clonogenic capacity

To determine if the expression of NE polypeptides initiating from internal translational start sites are harmful to cells, we expressed cDNAs containing internal ORFs in U937 promonocytes, performing a previously described "clonogenic capacity" assay, developed to study neutropenia-associated *ELANE* mutation induction of the UPR.[21] Three different vectors were used in order to isolate the different ORFs and determine their effects; in addition to expressing the ATG2 ORF and the ATG3 ORF, we also evaluated the ATG>GTG mutation, which produces all 3 internal ORFs. (We did not test ORF4 individually, because its production seems

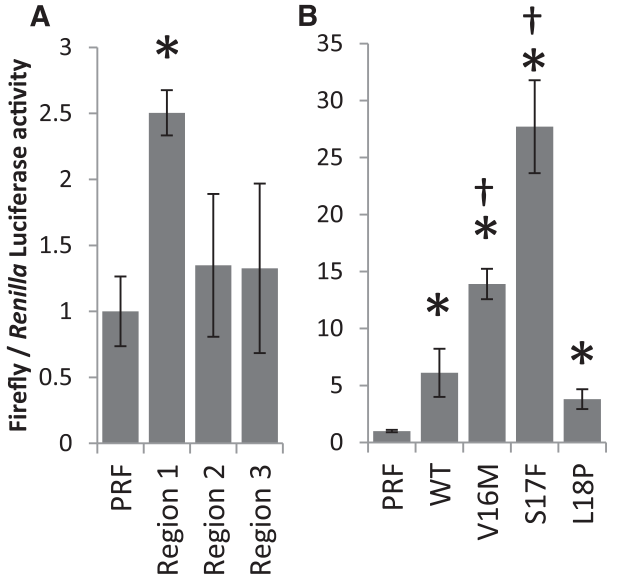

Figure 3. IRES activity from fragments of *ELANE* mRNA. (A) Activity from 3 overlapping regions of *ELANE* mRNA. Only region 1 showed an increase in IRES activity. Region 1: nt 171-233; Region 2: nt 42-233; and Region 3: nt 1-233 (NM_001972.2). (B) Activity from 3 tandem repeats of nt 171-193 of *ELANE*, either wild-type or mutant sequence. Data shown are mean ± standard deviation of 3 independent experiments. *$P < .05$ vs PRF; †$P < .05$ vs WT. WT, wild-type.

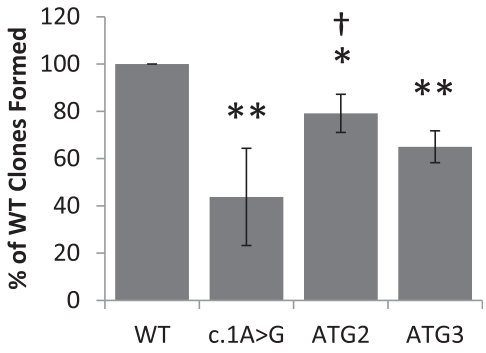

Figure 4. Clonogenic capacity of U937 cells transfected with *ELANE* vectors. Cells transfected with c.1A>G, ATG2 ORF, and ATG 3 ORF all formed significantly fewer clones. A total of 384 wells were counted for each group during each experiment. Data shown are mean ± standard deviation of 3 independent experiments. *$P < .05$ vs WT; **$P < .005$ vs WT; †$P = .05$ vs c.1A>G.

to require upstream sequences, and, in isolation, does not produce detectable protein.) All of the vectors expressing shortened forms of NE reduced clonogenic capacity (Figure 4). When comparing the shorter isoforms of NE to each other, the GTG mutation, which leads to production of all 3 internal ORFs, had a greater effect on inhibiting clonogenic capacity than did the ATG2 ORF by itself.

Cellular and biochemical properties of amino-terminally truncated NE

To determine if amino-terminally truncated forms of NE retain enzymatic activity, we tested their ability to cleave the NE-specific substrate MeO-Suc-Ala-Ala-Pro-Val-pNA following expression in transfected RBL-1 cells. We found that the c.1A>G mutation retained minimal, yet statistically significant residual activity, but that isolated ORFs corresponding to the second and third ATGs lacked activity (Figure 5A and supplemental Figure 6).

We assessed whether amino-terminally truncated forms of NE induce ER stress by measuring expression of *HSPA5*, which codes for the binding immunoglobulin protein. We found no increase in *HSPA5* in HL-60 cells transfected with *ELANE* mutations altering the translational start site (Figure 5B), whereas control cells transfected with wild-type *ELANE* and stimulated with tunicamycin, which induces ER stress,[21] showed a 12-fold increase in *HSPA5* expression (supplemental Figure 7).

We also tested whether amino-terminally truncated forms of NE induce apoptosis in HL-60 cells transfected with vectors expressing either wild-type or amino-terminally truncated forms of NE. There was no increase in apoptosis as observed by Annexin V binding (Figure 5C and supplemental Figure 8). Additionally, reverse transcription (transcriptase)-PCR assays revealed no increase in expression across a panel of apoptosis-related genes (supplemental Figure 9). The fact that apoptosis was evident in iPSC exposes the limitations of HL-60 cells.

To determine if amino-terminally truncated forms of NE subcellularly mislocalize, we transfected RBL-1 cells with the c.1A>G and c.3G>A mutations. Compared with granular cytoplasmic distribution of the wild-type, the shorter polypeptides appeared to localize to nuclei (supplemental Figure 10).

Discussion

Somatic and germline mutations of translational start sites are reported for several human disease-associated genes, where it is speculated that, instead of abrogating translation, they may force utilization of downstream initiation codons.[35,36] However, the demonstration of this phenomenon has been rare. One example involved acquired mutations of the hematopoietic transcription factor GATA1 associated with transient myeloproliferative disorder and megakaryoblastic leukemia of Down syndrome.[37] Start codon mutations or, more often, proximal chain-terminating mutations just downstream from the initiation codon, lead to the production of a shorter GATA1 variant commencing from a second initiation codon, which lacks the activation domain yet retains the ability to bind DNA and cofactors.[38,39] Similar mutations producing similar effects occur in the transcription factor C/EBPα in acute myeloid leukemia.[40] Another example involved germline mutation of *TPO*, encoding thrombopoietin, in hereditary thrombocytopenia, and disrupting a splice-site, which leads to deletion of the canonical start site with initiation shifting downstream to the next in-frame ATG codon.[41] Here, we show that neutropenia-associated germline mutations disrupt the initial ATG codon, and adjacent noncoding Kozak translation initiation sequence of *ELANE* lead to production of amino-terminally truncated isoforms of NE-initiating translation from downstream, in-frame methionine ATG codons.

Potential alternate translation start sites are predicted for as many as 12% of human genes.[42] Furthermore, potential alternate start sites are evolutionarily conserved and are used in many cases.[43-45]

One of the hypothesized roles of alternate translation start sites is to alter amino terminal localization signals, and ultimately, protein location; 30% of proteins derived from potential alternate start sites are predicted to have different subcellular localization.[42] One example is neuropeptide Y, which has two translation start sites. The protein produced from the first initiation codon is targeted to secretory vesicles whereas the protein initiating downstream locates to mitochondria.[46] We have shown that, at least in vitro, pathogenic isoforms of NE resulting from start-site mutations similarly become mislocalized when truncated at the amino terminus, probably because the shorter isoforms lack the ER-localizing signal sequence.

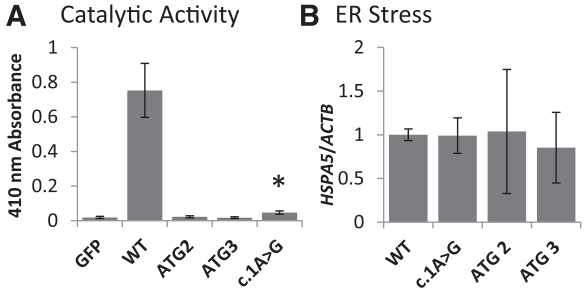

C Apoptosis

Vector	75.9 ±	3.39
WT	67.75 ±	0.49
c.1A>G	57.95 ±	13.65
ATG2	63.55 ±	1.48
ATG3	60.75 ±	9.69

Figure 5. Properties of amino-terminally truncated NE. (A) Mutant forms of NE are unable to cleave MeO-Suc-Ala-Ala-Pro-Val-pNA, an NE-specific substrate after a 16 hour incubation, except for c.1A>G which showed minimal residual activity. Data shown are mean ± standard deviation of 3 independent experiments. (B) No significant difference in ER stress was observed, as measured by *HSPA5* expression. Data shown are mean ± standard deviation of 3 independent experiments. (C) There is no observed increase in apoptosis, as measured by Annexin V staining. Mean ± standard deviations of 2 independent experiments are shown. *$P < .05$ vs GFP.

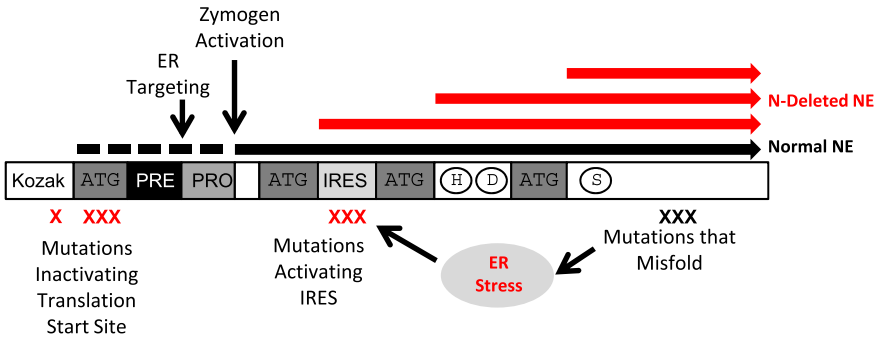

Figure 6. Congruence with current disease hypotheses. A schematic of *ELANE* is shown. Mutations that inactivate the translation initiation codon and the Kozak sequence force translation to initiate from downstream in-frame ATG codons, resulting in amino-terminally truncated NE that lacks an ER-localizing presignal sequence, as well as a pro-zymogen sequence ordinarily restraining proteolytic activity prior to its removal. A second group of mutations may activate an IRES, also leading to translation of the internal ORFs. A third type of mutation, we speculate, may cause protein misfolding which activates an ER stress response and promotes IRES utilization, thereby indirectly also leading to translation of the internal ORFs. Catalytic triad of his, asp, and ser residues and amino terminal sequences ordinarily cleaved from the mature enzyme (dotted line) are shown.

We demonstrated IRES activity for a region of *ELANE* between the second and third internal ATG codons. Based on prior studies of *Nkx6-2*, we suspected this activity was due to direct ribosomal binding mediated by *ELANE* mRNA sequence complementarity to 18S rRNA.[47] This IRES permits the production of both the ATG2 and ATG3 ORF NE polypeptides from a single mRNA when the initial ATG codon is mutated. It is less clear if this IRES normally initiates translation when the initial ATG codon or flanking Kozak sequence is not altered. Another interesting observation was that mutations of this region enhanced activity despite reducing complementarity to 18S rRNA compared with wild-type. In previous studies, it was found that the optimum length of complementarity to 18S rRNA was 7 nucleotides, and any sequence longer or shorter than that, decreased IRES activity.[48]

It is likely that other coding sequences within *ELANE* mRNA contribute to translational regulation directly either by influencing binding to the ribosome or other translation factors, or indirectly by affecting mRNA folding. If so, some coding sequence *ELANE* mutations may favor production of internally translated isoforms, in which case, protein sequence changes could prove incidental and non-contributory to pathogenesis. Conversely, *ELANE* variants involving synonymous codon substitutions that do not alter coding sequence may nevertheless prove pathogenic, because they disturb the translational start site, IRES, or other mRNA sequences regulating translation from internal start sites in *ELANE*. In our own genetic testing of neutropenic patients, we have detected novel synonymous *ELANE* variants, but have not previously designated them as deleterious.[1]

ELANE mutations inactivating the ATG initiation codon are found in SCN patients and lead to the absence of full-length protein with expression of amino-terminally truncated isoforms not seen with the wild-type allele. However, the Kozak sequence mutation occurs in patients with cyclic neutropenia and results in the production of both full-length protein, and compared with SCN patients, reduced levels of the amino-terminally truncated isoforms, suggesting that less expression of the shortened isoforms correlates with what might be considered, milder disease.

The shortened isoforms reduced clonogenic capacity in an assay of myeloid proliferation. Cells transfected with the shorter forms of NE did not exhibit increases in ER stress when compared with wild-type. It is not surprising that the mutations did not induce ER stress since they were predicted to lack the signal sequence necessary to translocate to the ER. However, the presence of a "smear" of high molecular weight products evident in western blots in Figure 2 and supplemental Figure 3E, suggested that the shortened forms of NE may still misfold and aggregate, albeit not in the ER. It is possible that aggregated NE may sequester transcription factors. ORFs 2 and 3 are additionally predicted to lack the pro-zymogen activation sequence whose removal is required for catalytic function; yet they retained the catalytic triad of histidine, aspartate, and serine necessary for proteolytic activity, raising the possibility that they were mature and possessed enzymatic activity immediately following translational synthesis. We found that mutation disrupting the canonical translation start site retained only minimal proteolytic activity; yet it is possible that even residual activity could be damaging if not properly compartmentalized.

In evaluating the relevance of this new category of mutations disrupting the translational start site, it is unlikely that all of the numerous *ELANE* mutations would disrupt translational regulation of mRNA and lead to production of internally translated ORFs. Nevertheless, we speculate that there may be a mechanism through which conventional mutations alter the primary sequence of NE, which may lead to the production of internally-translated isoforms via protein misfolding.

The presence of shorter isoforms of *ELANE* generated by an IRES, actually fits with the two current models on how mutations may cause disease (Figure 6). If the misfolding hypothesis holds true, the shorter isoforms could be produced by the IRES through a *trans* mechanism. In times of stress, protein misfolding within the ER activates PERK, which phosphorylates eukaryotic translation initiation factor 2,[49] resulting in a preference for IRES-mediated translation over normal cap-dependent translation.[50] Our observations also fit well with the mislocalization hypothesis. Since the shortened isoforms do not contain a propeptide signal sequence, they are unlikely to correctly transit through the ER, where they would ordinarily become glycosylated. Previously, we demonstrated that when sites of asparagine-linked glycosylation in NE are mutated, NE accumulates in the nucleus.[25] In fact, the shorter isoforms appear to localize to the nucleus in RBL-1 cells, congruent with the theory that they do not enter the ER and are not glycosylated. Aberrant localization may contribute to pathogenesis, but further research is needed to establish if this is also true in human neutrophils and what link it may have to disease.

Acknowledgments

This work was supported by research grants from the National Institutes of Health (R01DK58161) and the US Department of Defense (BM120152).

Authorship

Contribution: T.T., J.W., and M.S.H. conceived and designed the study; H.L.G., C.L., and J.A.C designed iPSC studies; T.T., J.W., S.J.C., H.L.G., C.L., J.A.C., and M.S.H. analyzed and interpreted the data; T.T. and M.S.H. wrote the paper; J.W. performed isoform expression and western blot experiments (except for iPSC); R.C.N. and L.T. performed iPSC studies; S.J.S. performed immunolocalization studies; T.T. performed all other studies with the assistance of J.W.; and S.J.C., T.G., J.C.C., and J.D. ascertained and clinically evaluated patients described here.

Conflict-of-interest disclosure: The authors declare no competing financial interests.

Correspondence: Marshall S. Horwitz, Department of Pathology, University of Washington School of Medicine, Box 358056, Seattle, WA 98195; e-mail: horwitz@uw.edu.

References

1. Horwitz MS, Corey SJ, Grimes HL, Tidwell T. ELANE mutations in cyclic and severe congenital neutropenia: genetics and pathophysiology. *Hematol Oncol Clin North Am.* 2013;27(1):19-41, vii. [vii.]
2. Horwitz M, Benson KF, Person RE, Aprikyan AG, Dale DC. Mutations in ELA2, encoding neutrophil elastase, define a 21-day biological clock in cyclic haematopoiesis. *Nat Genet.* 1999;23(4):433-436.
3. Dale DC, Person RE, Bolyard AA, et al. Mutations in the gene encoding neutrophil elastase in congenital and cyclic neutropenia. *Blood.* 2000; 96(7):2317-2322.
4. Klein C, Grudzien M, Appaswamy G, et al. HAX1 deficiency causes autosomal recessive severe congenital neutropenia (Kostmann disease). *Nat Genet.* 2007;39(1):86-92.
5. Person RE, Li FQ, Duan Z, et al. Mutations in proto-oncogene GFI1 cause human neutropenia and target ELA2. *Nat Genet.* 2003;34(3):308-312.
6. Boztug K, Appaswamy G, Ashikov A, et al. A syndrome with congenital neutropenia and mutations in G6PC3. *N Engl J Med.* 2009;360(1): 32-43.
7. Boztug K, Klein C. Genetics and pathophysiology of severe congenital neutropenia syndromes unrelated to neutrophil elastase. *Hematol Oncol Clin North Am.* 2013;27(1):43-60.
8. Korkmaz B, Horwitz MS, Jenne DE, Gauthier F. Neutrophil elastase, proteinase 3, and cathepsin G as therapeutic targets in human diseases. *Pharmacol Rev.* 2010;62(4):726-759.
9. Germeshausen M, Deerberg S, Peter Y, Reimer C, Kratz CP, Ballmaier M. The spectrum of ELANE mutations and their implications in severe congenital and cyclic neutropenia. *Hum Mutat.* 2013;34(6):905-914.
10. Köllner I, Sodeik B, Schreek S, et al. Mutations in neutrophil elastase causing congenital neutropenia lead to cytoplasmic protein accumulation and induction of the unfolded protein response. *Blood.* 2006;108(2):493-500.
11. Li FQ, Horwitz M. Characterization of mutant neutrophil elastase in severe congenital neutropenia. *J Biol Chem.* 2001;276(17): 14230-14241.
12. Benson KF, Li FQ, Person RE, et al. Mutations associated with neutropenia in dogs and humans disrupt intracellular transport of neutrophil elastase. *Nat Genet.* 2003;35(1):90-96.
13. Massullo P, Druhan LJ, Bunnell BA, et al. Aberrant subcellular targeting of the G185R neutrophil elastase mutant associated with severe congenital neutropenia induces premature apoptosis of differentiating promyelocytes. *Blood.* 2005;105(9):3397-3404.
14. Dell'Angelica EC, Shotelersuk V, Aguilar RC, Gahl WA, Bonifacino JS. Altered trafficking of lysosomal proteins in Hermansky-Pudlak syndrome due to mutations in the beta 3A subunit of the AP-3 adaptor. *Mol Cell.* 1999;3(1):11-21.
15. Meng R, Bridgman R, Toivio-Kinnucan M, et al. Neutrophil elastase-processing defect in cyclic hematopoietic dogs. *Exp Hematol.* 2010;38(2): 104-115.
16. Introne W, Boissy RE, Gahl WA. Clinical, molecular, and cell biological aspects of Chediak-Higashi syndrome. *Mol Genet Metab.* 1999;68(2): 283-303.
17. Cavarra E, Martorana PA, Cortese S, Gambelli F, Di Simplicio P, Lungarella G. Neutrophils in beige mice secrete normal amounts of cathepsin G and a 46 kDa latent form of elastase that can be activated extracellularly by proteolytic activity. *Biol Chem.* 1997;378(5):417-423.
18. El Chehadeh S, Aral B, Gigot N, et al. Search for the best indicators for the presence of a VPS13B gene mutation and confirmation of diagnostic criteria in a series of 34 patients genotyped for suspected Cohen syndrome. *J Med Genet.* 2010; 47(8):549-553.
19. Stepensky P, Saada A, Cowan M, et al. The Thr224Asn mutation in the VPS45 gene is associated with the congenital neutropenia and primary myelofibrosis of infancy. *Blood.* 2013; 121(25):5078-5087.
20. Vilboux T, Lev A, Malicdan MC, et al. A congenital neutrophil defect syndrome associated with mutations in VPS45. *N Engl J Med.* 2013;369(1): 54-65.
21. Grenda DS, Murakami M, Ghatak J, et al. Mutations of the ELA2 gene found in patients with severe congenital neutropenia induce the unfolded protein response and cellular apoptosis. *Blood.* 2007;110(13):4179-4187.
22. Julier C, Nicolino M. Wolcott-Rallison syndrome. *Orphanet J Rare Dis.* 2010;5:29.
23. Nanua S, Murakami M, Xia J, et al. Activation of the unfolded protein response is associated with impaired granulopoiesis in transgenic mice expressing mutant Elane. *Blood.* 2011;117(13): 3539-3547.
24. Chappell SA, Edelman GM, Mauro VP. A 9-nt segment of a cellular mRNA can function as an internal ribosome entry site (IRES) and when present in linked multiple copies greatly enhances IRES activity. *Proc Natl Acad Sci USA.* 2000; 97(4):1536-1541.
25. Salipante SJ, Rojas ME, Korkmaz B, et al. Contributions to neutropenia from PFAAP5 (N4BP2L2), a novel protein mediating transcriptional repressor cooperation between Gfi1 and neutrophil elastase. *Mol Cell Biol.* 2009; 29(16):4394-4405.
26. Melkonyan H, Sorg C, Klempt M. Electroporation efficiency in mammalian cells is increased by dimethyl sulfoxide (DMSO). *Nucleic Acids Res.* 1996;24(21):4356-4357.
27. Bellanné-Chantelot C, Clauin S, Leblanc T, et al. Mutations in the ELA2 gene correlate with more severe expression of neutropenia: a study of 81 patients from the French Neutropenia Register. *Blood.* 2004;103(11):4119-4125.
28. Setty BA, Yeager ND, Bajwa RP. Heterozygous M1V variant of ELA-2 gene mutation associated with G-CSF refractory severe congenital neutropenia. *Pediatr Blood Cancer.* 2011;57(3): 514-515.
29. Nakagawa S, Niimura Y, Gojobori T, Tanaka H, Miura K. Diversity of preferred nucleotide sequences around the translation initiation codon in eukaryote genomes. *Nucleic Acids Res.* 2008; 36(3):861-871.
30. Abecasis GR, Altshuler D, Auton A, et al. A map of human genome variation from population-scale sequencing. The 1000 Genomes Project Consortium. *Nature.* 2010;467(7319):1061-1073.
31. Sherry ST, Ward MH, Kholodov M, et al. dbSNP: the NCBI database of genetic variation. *Nucleic Acids Res.* 2001;29(1):308-311.
32. Gullberg U, Lindmark A, Lindgren G, Persson AM, Nilsson E, Olsson I. Carboxyl-terminal prodomain-deleted human leukocyte elastase and cathepsin G are efficiently targeted to granules and enzymatically activated in the rat basophilic/mast cell line RBL. *J Biol Chem.* 1995;270(21): 12912-12918.
33. Gilbert WV. Alternative ways to think about cellular internal ribosome entry. *J Biol Chem.* 2010;285(38):29033-29038.
34. Dresios J, Chappell SA, Zhou W, Mauro VP. An mRNA-rRNA base-pairing mechanism for translation initiation in eukaryotes. *Nat Struct Mol Biol.* 2006;13(1):30-34.
35. Kozak M. Emerging links between initiation of translation and human diseases. *Mamm Genome.* 2002;13(8):401-410.
36. Wolf A, Caliebe A, Thomas NS, et al. Single base-pair substitutions at the translation initiation sites of human genes as a cause of inherited disease. *Hum Mutat.* 2011;32(10):1137-1143.
37. Tsai MH, Hou JW, Yang CP, et al. Transient myeloproliferative disorder and GATA1 mutation in neonates with and without Down syndrome. *Indian J Pediatr.* 2011;78(7):826-832.
38. Wechsler J, Greene M, McDevitt MA, et al. Acquired mutations in GATA1 in the megakaryoblastic leukemia of Down syndrome. *Nat Genet.* 2002;32(1):148-152.
39. Rainis L, Bercovich D, Strehl S, et al. Mutations in exon 2 of GATA1 are early events in megakaryocytic malignancies associated with trisomy 21. *Blood.* 2003;102(3):981-986.
40. Paz-Priel I, Friedman A. C/EBPα dysregulation in AML and ALL. *Crit Rev Oncog.* 2011;16(1-2): 93-102.
41. Wiestner A, Schlemper RJ, van der Maas AP, Skoda RC. An activating splice donor mutation in the thrombopoietin gene causes hereditary thrombocythaemia. *Nat Genet.* 1998;18(1):49-52.
42. Kochetov AV, Sarai A, Rogozin IB, Shumny VK, Kolchanov NA. The role of alternative translation start sites in the generation of human protein diversity. *Mol Genet Genomics.* 2005;273(6):491-496.
43. Bazykin GA, Kochetov AV. Alternative translation start sites are conserved in eukaryotic genomes. *Nucleic Acids Res.* 2011;39(2):567-577.

44. Kochetov AV. Alternative translation start sites and hidden coding potential of eukaryotic mRNAs. *Bioessays*. 2008;30(7): 683-691.

45. Fritsch C, Herrmann A, Nothnagel M, et al. Genome-wide search for novel human uORFs and N-terminal protein extensions using ribosomal footprinting. *Genome Res*. 2012; 22(11):2208-2218.

46. Kaipio K, Kallio J, Pesonen U. Mitochondrial targeting signal in human neuropeptide Y gene. *Biochem Biophys Res Commun*. 2005;337(2): 633-640.

47. Hu MC, Tranque P, Edelman GM, Mauro VP. rRNA-complementarity in the 5′ untranslated region of mRNA specifying the Gtx homeodomain protein: evidence that base- pairing to 18S rRNA affects translational efficiency. *Proc Natl Acad Sci USA*. 1999;96(4):1339-1344.

48. Chappell SA, Edelman GM, Mauro VP. Biochemical and functional analysis of a 9-nt RNA sequence that affects translation efficiency in eukaryotic cells. *Proc Natl Acad Sci USA*. 2004; 101(26):9590-9594.

49. Wek RC, Cavener DR. Translational control and the unfolded protein response. *Antioxid Redox Signal*. 2007;9(12):2357-2371.

50. Fernandez J, Yaman I, Sarnow P, Snider MD, Hatzoglou M. Regulation of internal ribosomal entry site-mediated translation by phosphorylation of the translation initiation factor eIF2alpha. *J Biol Chem*. 2002;277(21): 19198-19205.

2014 123: 562-569
doi:10.1182/blood-2013-07-513242 originally published online November 1, 2013

Neutropenia-associated *ELANE* mutations disrupting translation initiation produce novel neutrophil elastase isoforms

Timothy Tidwell, Jeremy Wechsler, Ramesh C. Nayak, Lisa Trump, Stephen J. Salipante, Jerry C. Cheng, Jean Donadieu, Taly Glaubach, Seth J. Corey, H. Leighton Grimes, Carolyn Lutzko, Jose A. Cancelas and Marshall S. Horwitz

Blood (print ISSN 0006-4971, online ISSN 1528-0020), is published weekly by the American Society of Hematology, 2021 L St, NW, Suite 900, Washington DC 20036.

Pathogenesis of *ELANE*-mutant severe neutropenia revealed by induced pluripotent stem cells

Ramesh C. Nayak,[1] Lisa R. Trump,[1] Bruce J. Aronow,[2] Kasiani Myers,[3] Parinda Mehta,[3] Theodosia Kalfa,[1] Ashley M. Wellendorf,[1] C. Alexander Valencia,[4] Patrick J. Paddison,[5] Marshall S. Horwitz,[6] H. Leighton Grimes,[1,7] Carolyn Lutzko,[1,8] and Jose A. Cancelas[1,8]

[1]Division of Experimental Hematology and Cancer Biology, [2]Division of Biomedical Informatics, [3]Division of Bone Marrow Transplantation and Immunodeficiencies, and [4]Human Genetics from the Department of Pediatrics, Cincinnati Children's Hospital Medical Center and University of Cincinnati College of Medicine, Cincinnati, Ohio, USA. [5]Department of Molecular and Cellular Biology, Fred Hutchinson Cancer Research Center, Seattle, Washington, USA. [6]Department of Pathology, University of Washington School of Medicine, Seattle, Washington, USA. [7]Division of Immunobiology, Cincinnati Children's Hospital Medical Center, Cincinnati, Ohio, USA. [8]Hoxworth Blood Center, University of Cincinnati College of Medicine, Cincinnati, Ohio, USA.

Severe congenital neutropenia (SCN) is often associated with inherited heterozygous point mutations in *ELANE*, which encodes neutrophil elastase (NE). However, a lack of appropriate models to recapitulate SCN has substantially hampered the understanding of the genetic etiology and pathobiology of this disease. To this end, we generated both normal and SCN patient–derived induced pluripotent stem cells (iPSCs), and performed genome editing and differentiation protocols that recapitulate the major features of granulopoiesis. Pathogenesis of *ELANE* point mutations was the result of promyelocyte death and differentiation arrest, and was associated with NE mislocalization and activation of the unfolded protein response/ER stress (UPR/ER stress). Similarly, high-dose G-CSF (or downstream signaling through AKT/BCL2) rescues the dysgranulopoietic defect in SCN patient–derived iPSCs through C/EBPβ-dependent emergency granulopoiesis. In contrast, sivelestat, an NE-specific small-molecule inhibitor, corrected dysgranulopoiesis by restoring normal intracellular NE localization in primary granules; ameliorating UPR/ER stress; increasing expression of *CEBPA*, but not *CEBPB*; and promoting promyelocyte survival and differentiation. Together, these data suggest that SCN disease pathogenesis includes NE mislocalization, which in turn triggers dysfunctional survival signaling and UPR/ER stress. This paradigm has the potential to be clinically exploited to achieve therapeutic responses using lower doses of G-CSF combined with targeting to correct NE mislocalization.

Introduction

Severe congenital neutropenia (SCN) is a rare myelopoietic disorder resulting in recurrent life-threatening infections due to a lack of mature neutrophils (1). Individuals with SCN have myeloid hypoplasia with arrest of myelopoiesis at the promyelocyte/myelocyte stage (2). Current treatment by administration of high-dose granulocyte CSF (G-CSF) induces an increase in the neutrophil counts in the peripheral blood (PB) of most SCN patients. The lack of beneficial effect of G-CSF administration on neutrophil function (3) and the possible role of G-CSF administration in leukemogenesis (4) underscores the need to search for alternative therapies. Currently, allogeneic hematopoietic stem cell transplantation (HSCT) is the only curative treatment for SCN (5).

SCN is actually a multigene syndrome that can be caused by inherited mutations in several genes. Around 60% of SCN patients are known to carry autosomal-dominant mutations in the *ELANE* gene, which encodes neutrophil elastase (NE) (6, 7). NE belongs to the class of serine proteases and is expressed exclusively in mature myelomonocytic cells and their committed immature precursors (promyelocytes and promonocytes). Stored as an active protease in azurophilic granules, NE is released upon exposure of the neutrophil to inflammatory stimuli. In the extracellular environment, NE cleaves extracellular matrix proteins, while serine protease inhibitors antagonize the proteinase activity (8).

Most *ELANE* mutations act as dominant heterozygous mutations and are single point mutations. It is unclear how these single point mutations affect the function of the protein and the viability of phagocytes. Some data suggest that *ELANE* gene mutations are not sufficient to cause the SCN phenotype and other genes may act as modifiers on promyelocyte survival and their response to G-CSF (9–11). There is also an absence of correlation between the genotype and phenotype. The same *ELANE* mutation can induce 2 types of disease: SCN and a more benign cyclic neutropenia, with cycles of neutropenia every 21 days (6). It is possible that disturbances of a feedback circuit, in which mature neutrophils homeostatically regulate myeloid progenitor populations, are responsible for this mechanism. This hypothesis was supported by the discovery that the protein PFAAP5 interacts with NE to interfere with GFI1-controlled transcriptional regulation (12). Finally, the coexistence of various phenotypes in the same kindred may point to the existence of modifying genes that determine the severity of the clinical phenotype (13).

Early explanations of the role of mutant *ELANE* portrayed a potential pathophysiological role of dysregulated vesicular sorting

Authorship note: Ramesh C. Nayak and Lisa R. Trump contributed equally to this manuscript. H. Leighton Grimes, Carolyn Lutzko, and Jose A. Cancelas are co-corresponding authors.
Conflict of interest: The authors have declared that no conflict of interest exists.
Submitted: January 12, 2015; **Accepted:** June 5, 2015.
Reference information: *J Clin Invest*. 2015;125(8):3103–3116. doi:10.1172/JCI80924.

and membrane trafficking (14) because canine cyclic neutropenia resulted from mutations in the gene that encodes a subunit of the AP3 adapter complex, which is involved in trafficking of proteins out of the Golgi complex (14). A number of indirect observations have also implicated aberrant stress response in the ER. The unfolded protein response (UPR) has evolved to protect cells from the damaging effects of improperly folded proteins. Nascent proteins destined for secretory vesicles are directed to the ER, where the protein folding takes place (15). Myeloid cell lines and primary human cells engineered to express mutant NE, as well as primary human cells from SCN patients with *ELANE* mutations, show increased biochemical evidence of UPR/ER stress (16, 17).

However, controversy about the pathogenetic mechanisms of this disease has extended over 20 years because neither in vitro myelopoeisis/granulopoiesis models, nor mouse models recapitulate the disease. Two different models of mutant *ELANE* knockin mice showed no neutropenia basally or after chemotherapy-induced stress (18, 19). One of these mice only developed neutropenia after administration of a potent proteasome inhibitor but not after silencing the most relevant UPR sensor, Perk (19). Lack of adequate modeling is compounded by the limited availability of hematopoietic progenitor materials from pediatric patients with a rare marrow-failure disorder.

The recent discovery that somatic cells can be reprogrammed to generate induced pluripotent stem cell lines (iPSC lines), and so provide a renewable source of patient-derived cells to study the cellular mechanisms of disease, has rejuvenated the application of the Koch postulate to genetic diseases that cannot be recapitulated in animal models (20). In SCN, the use of iPSCs has provided evidence of canonical Wnt signaling in disease pathogenesis (21). However, a lack of targeted therapies against Wnt signaling has limited the clinical application of this knowledge in the therapy of *ELANE*-mutant SCN. Our group has recently demonstrated the utility of iPSC-derived myelopoiesis models to identify the pathogenetic mechanisms of unusual *ELANE* mutations that affect NE translation (22). Here, by characterizing iPSC-derived granulopoiesis from SCN patients with *ELANE* mutations and isogenic lines generated by gene repair, we resolve the necessity of the *ELANE* mutation in SCN dysgranulopoiesis. Moreover, our modeling reveals the molecular details underlying SCN disease pathogenesis, linking the concepts of NE mislocalization with the induction of UPR/ER stress. We show that while high-dose G-CSF therapy rescues SCN iPSC–derived promyelocytes through C/EBPβ-dependent emergency granulopoiesis, the application of low-dose G-CSF with a small-molecule NE-protease inhibitor restores normal intracellular NE localization in primary granules, ameliorates UPR/ER stress, facilitates promyelocyte survival, and restores *CEBPA* expression and granulocyte differentiation. Our results underscore a central role for NE mislocalization in SCN pathogenesis and provide proof-of-principle for therapeutic intervention exploiting NE protein relocalization.

Results

SCN patient iPSC–derived myeloid progenitors display impaired granulocytic differentiation. In the present study, we developed iPSCs from the PB of 2 healthy subjects (control 12 and control 13), and 2 children with *ELANE* mutations ($ELANE^{Q97P}$ named SCN14 and $ELANE^{I118N}$ named SCN15). These 2 patients were chosen because of the severity of their congenital neutropenia at diagnosis, including maintained polymorphonuclear cell counts (PMN cell counts) < 500/mm^3, and both showed BM maturation arrest at the myelocytic/metamyelocytic stage with no segmented neutrophils and relative marrow eosinophilia and monocytosis. In addition, both patients responded to only high doses of G-CSF (SCN14 derives from a patient requiring 8 μg/kg/day, and SCN15 derives from a patient requiring 5 μg/kg/day to maintain PMN counts > 1,000/mm^3), which represents a frequent event in mutant-*ELANE* SCN.

Upon transduction of PB mononuclear cells (MNCs) with Yamanaka factors in a lentiviral construct, pluripotent stem cell–like colonies appeared on the culture plate 10–15 days following transduction. The SCN iPSC lines retained their SCN point mutations after reprogramming (Supplemental Figure 1; supplemental material available online with this article; doi:10.1172/JCI80924DS1) and remained karyotypically normal throughout culture (data not shown). All iPSC lines expressed the pluripotent markers SSEA-4, Tra-1-60, Tra-1-81, CD9, and OCT-4 as analyzed by flow cytometry (Supplemental Figure 2). To investigate the ability of iPSC lines to differentiate into hematopoietic cells, we used a 10-day monolayer differentiation protocol to produce $CD45^+CD34^+$ hematopoietic progenitors (23). At the end of the monolayer differentiation protocol, the generated cells were analyzed for CD45 and CD34 expression by FACS analysis. All iPSC lines were able to differentiate into hematopoietic progenitor cells as assessed by the frequency of $CD45^+CD34^+$ cells at the end of 10 days of differentiation (control 12, 34.9% ± 11.21%; control 13, 23.4% ± 7.8%; SCN15, 17.5% ± 5.2%; SCN14, 38.8% ± 8.9%) (Supplemental Figure 3A). $CD45^+CD34^+$ cells from these cultures also expressed CD33 and CD43, indicating that these are myeloid progenitor cells derived from primitive hematopoiesis (Supplemental Figure 3, B). For the functional analyses of these myeloid progenitor cells derived from control iPSCs and *ELANE*-mutant SCN iPSCs, we carried out CFU assays using semisolid methyl cellulose medium containing cytokine mixtures for myeloid cells. As shown in Figure 1A, hematopoietic progenitor cells derived from the 2 *ELANE*-mutant SCN iPSC lines generated approximately 75% and 50% reduction in CFU-G (granulocyte) and CFU-GM (granulocyte-macrophage) colonies, respectively, in comparison to that of control iPSC–derived hematopoietic progenitor cells. However, both the SCN iPSC–derived hematopoietic progenitor cells increased modestly the generation of CFU-M (macrophagic) in SCN15. The frequency of immature CFU-Mix generated from these cultures was comparable among all the lines. The colonies were plucked, stained with Wright-Giemsa and analyzed for the presence of myeloid differentiated cells. Histologic analysis of CFU-G derived from control iPSC hematopoietic progenitors confirmed the colonies contained mature neutrophils. CFU-G colonies derived from *ELANE*-mutant SCN lines were smaller (controls: 835.7 μm ± 172.5 μm vs. *ELANE* mutant: 328.5 μm ± 121.9 μm; Supplemental Figure 4, A and B) and were mostly composed of immature myeloid cells, mainly promyelocytes and myelocytes, and a few bands and neutrophils. The CFU-GM colonies derived from the control iPSC hematopoietic progenitor cells contained mature neutrophils and macrophages. However, *ELANE*-mutant

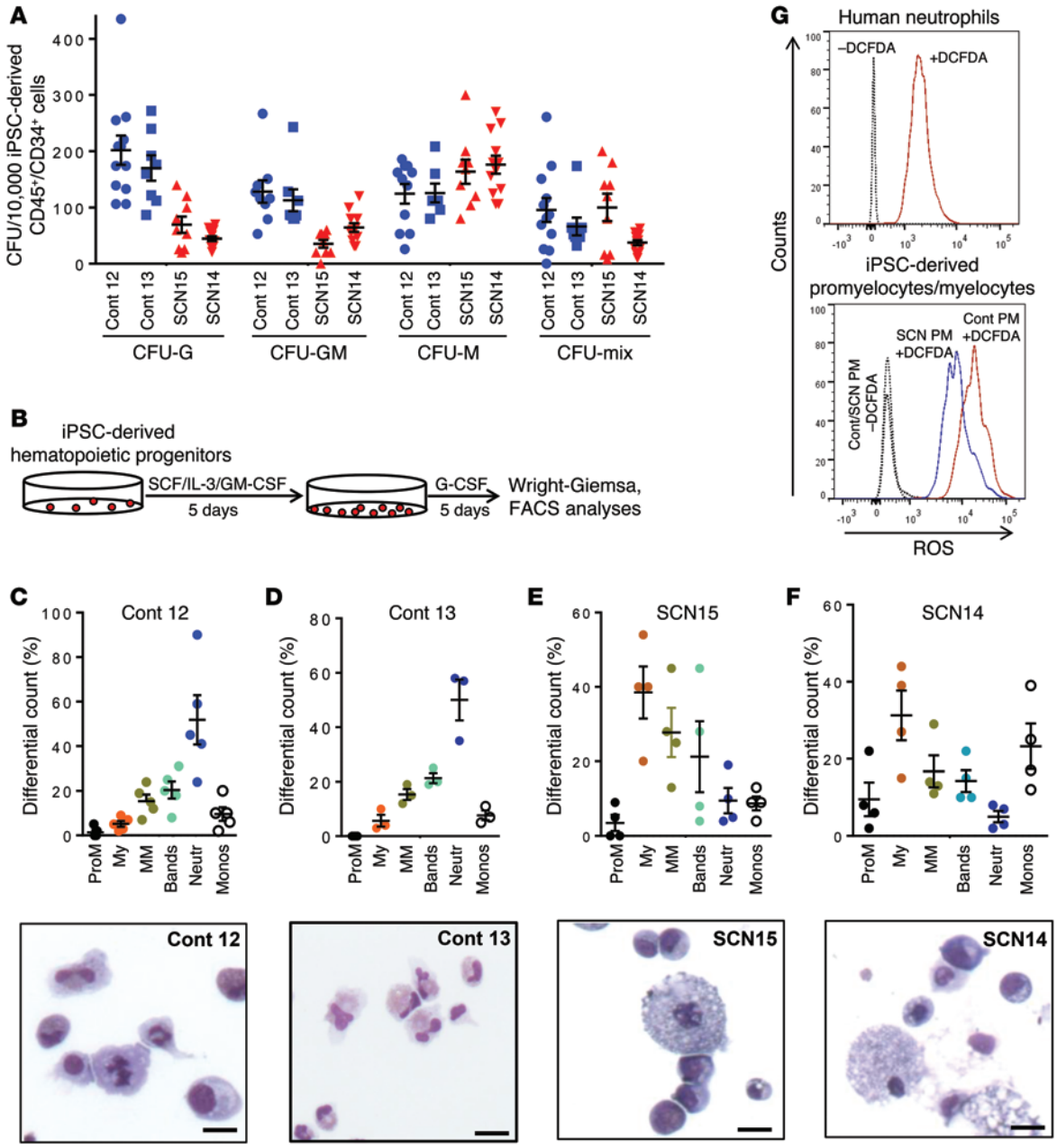

Figure 1. Impaired granulopoietic differentiation of hematopoietic progenitors derived from SCN patient iPSCs. (**A**) Colony forming cell assay of the hematopoietic progenitors derived from healthy donor (control 12 and control 13) and *ELANE*-mutant SCN iPSCs (SCN15 and SCN14). Cells were cultured in methyl cellulose semisolid medium with cytokines, and the myeloid (CFU-G, CFU-GM, CFU-M) and mix colonies were scored at day 14. (**B**) Schematic diagram of granulopoietic differentiation of iPSC-derived hematopoietic progenitors. (**C**) Top: Quantitative analyses of the granulopoietic differentiation of control iPSC–derived (control 12–derived) hematopoietic progenitors in liquid culture with myeloid differentiation cytokines. Bottom: Wright-Giemsa–stained cytospin at the end of the culture. (**D**) Top: Quantitative analyses of the granulopoietic differentiation of control iPSC–derived (control 13–derived) hematopoietic progenitors in liquid culture with myeloid differentiation cytokines. Bottom: Wright-Giemsa–stained cytospin at the end of the culture. (**E**) Top: Quantitative analyses of the granulopoietic differentiation of hematopoietic progenitors derived from SCN15 iPSCs in liquid culture condition with myeloid differentiation cytokines. Bottom: Wright-Giemsa–stained cytospin at the end of the culture. (**F**) Top: Quantitative analyses of the granulopoietic differentiation of hematopoietic progenitors derived from SCN14 iPSCs in liquid culture with myeloid differentiation cytokines. Bottom: Wright-Giemsa–stained cytospin at the end of the culture. (**G**) FACS-based ROS-generating-activity analyses of promyelocytes derived from control and SCN iPSCs. Scale bars: 10 μm. ProM, promyelocytes; My, myelocytes; MM, metamyelocytes; Neutr, neutrophils; Monos, monocytes. Data are presented as mean ± SD of individual values out of 4 or 5 independent experiments. Cont, control.

SCN iPSC–derived CFU-GM colonies lacked mature neutrophils and mainly contained macrophage and immature myeloid cells. The CFU-M colonies from both control and SCN iPSCs contained macrophages (Supplemental Figure 4, A and B).

For the precise quantitation of granulocytic lineage populations, granulopoietic differentiation of myeloid progenitor cells derived from control iPSCs and *ELANE*-mutant SCN iPSCs was performed in a 2-step liquid culture (Figure 1B). At the end of cul-

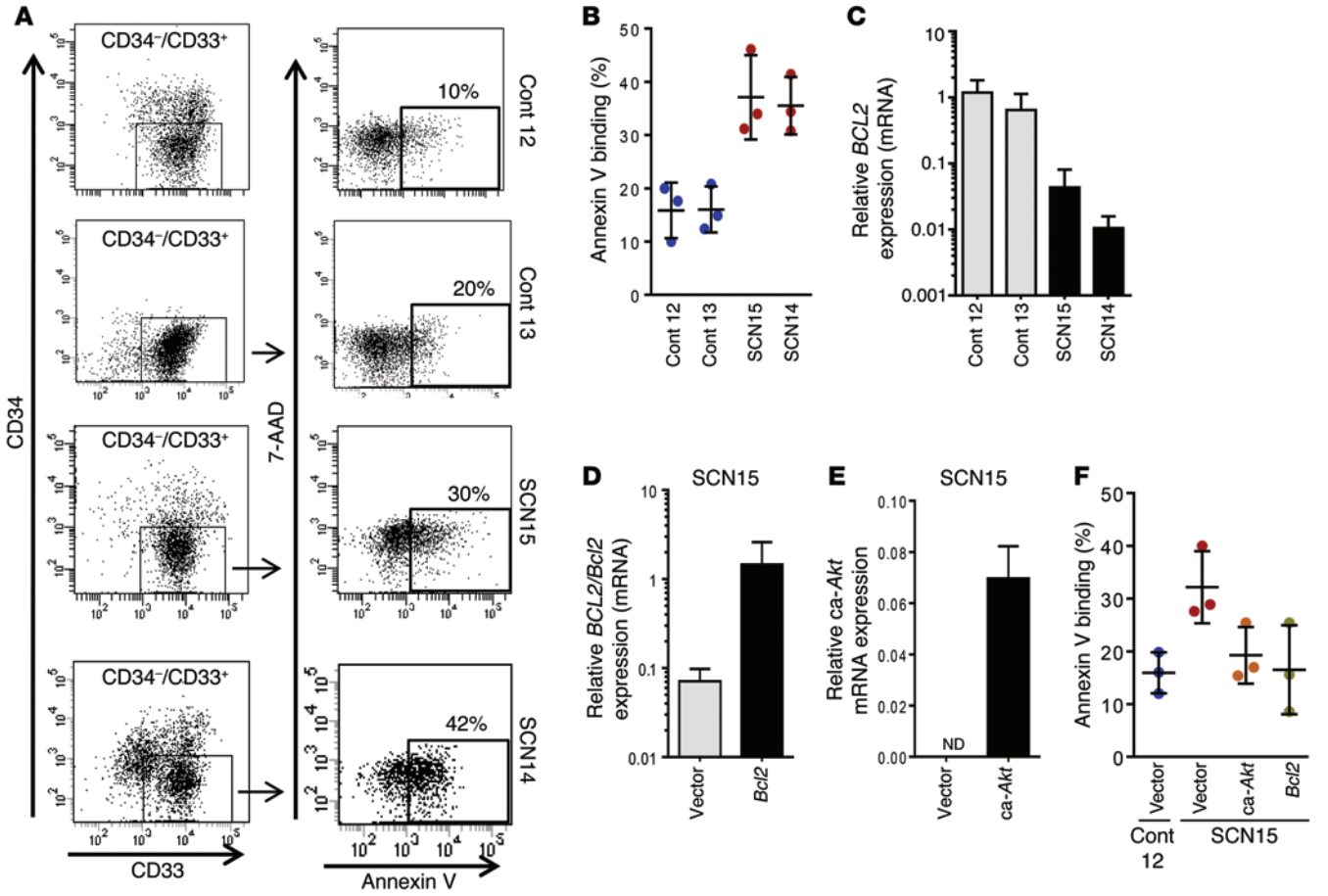

Figure 2. Defective differentiation of promyelocytes derived from SCN iPSCs is associated with apoptosis, which can be reversed by forced activation of Akt/Bcl2. (**A**) FACS dot plot showing annexin V binding on myeloid precursors derived from control (control 12 and control 13), *ELANE*-mutant SCN iPSCs (SCN15 and SCN14). (**B**) Quantitation of the % annexin V binding. (**C**) Relative expression of *BCL2* in promyelocytes derived from control and SCN iPSCs. (**D**) Ectopic expression of murine Bcl2 through retroviral transduction of myeloid precursors derived from SCN iPSCs (SCN15). (**E**) Ectopic expression of ca-Akt through retroviral transduction of myeloid precursors derived from SCN iPSCs (SCN15). (**F**) Quantitation of annexin V binding in control-, ca-Akt–, or Bcl2-expressing granulocytic precursors derived from SCN iPSCs. For **B** and **F**, data are presented as mean ± SD of 3 independent experiments. For **C**–**E**, data are presented as mean ± SD of 2 or more independent experiments in duplicate. Cont, control.

ture, stages of differentiation were identified by morphological analysis. As shown in Figure 1, C and D, the control iPSC–derived myeloid progenitors differentiated into monocytes and increasing frequencies of differentiated neutrophils and bands. Comparative transcriptome analysis of iPSCs; iPSC-differentiated mesoderm (24); myeloid progenitors (day 10 $CD45^+CD34^+CD33^+$ cells); and precursors (day 15 $CD45^+CD34^-CD33^+CD11b^-CD15^{+/low}$ cells) demonstrated that the myeloid progenitors and precursors were distinctly different from undifferentiated iPSCs and mesoderm-committed iPSCs. The expression of a total of 1,028 genes representing the iPSC signature is downregulated at a similar level in iPSC-derived myeloid progenitors and precursors as their primary BM myeloid progenitor and precursor counterparts. The expression of 828 hematopoietic genes was found to be upregulated in BM- or iPSC-derived myeloid progenitors and precursors. Pathway analysis using gene ontology analysis demonstrated that most of the upregulated genes were implicated in innate immunity and granulocyte physiology functions (clusters 6 and 7 of Supplemental Figure 5), and there were no major differences in the transcriptomes of primary BM myeloid progenitors or precursors and their iPSC-derived counterparts (Supplemental Figure 5). These data suggest that the expression of iPSC-derived and endogenous BM–derived myelopoiesis follow similar patterns.

Interestingly, the granulocytic population generated from *ELANE*-mutant SCN iPSC–derived myeloid progenitors is shifted to the left with myelocytes as the most frequently represented cell population and a largely reduced level of bands and neutrophils. These data suggest that *ELANE*-mutant SCN iPSC–derived myeloid progenitor cells are arrested at the myelocyte stage of granulopoietic development (Figure 1, E–F). These results mimic the precursor arrest at the myelocyte/metamyelocyte level of the BM at diagnosis from the patients from which iPSC lines were derived (data not shown). The FACS analyses of granulopoietic differentiation of control and SCN iPSC–derived cells show increased accumulation of promyelocytes/myelocytes ($CD45^+CD34^-CD33^+CD11b^-CD15^{+/low}$) in SCN iPSC–derived cells (Supplemental Figure 6). There was an increased percentage of monocytes observed in the case of the SCN14-derived myelopoietic cultures (Figure 1F). Monocytopoiesis in these cultures correlates with absolute monocytosis (25) in primary cultures of BM progenitors (26) in SCN

patients. The generation of reactive oxygen species (ROS) is a major functional hallmark of granulocytic lineage. Therefore, we analyzed the ROS production ability of granulocytic differentiated cells derived from control and SCN iPSC myeloid progenitors. Since the SCN iPSC–derived myeloid progenitor cells are arrested at the myelocyte stage, we analyzed the ability of promyelocytes/myelocytes derived from control or SCN iPSC myeloid progenitors to produce ROS following staining with dichlorofluorescin diacetate (DCFDA) and analysis by FACS. As shown in Figure 1G, the ROS-generating ability of SCN iPSC–derived promyelocytes/myelocytes is reduced compared with that of control iPSC–derived cells. All these results suggest that the *ELANE* SCN iPSC–derived hematopoietic progenitor cells can be used as a bona fide resource to study the pathophysiology of severe congenic neutropenia disease at molecular and cellular levels.

ELANE-mutant SCN iPSC–derived myeloid precursor cells undergo apoptosis that can be rescued by forced expression of active Akt or Bcl2. We investigated the underlying mechanisms of the impaired neutrophil development of *ELANE*-mutant SCN iPSC–derived myeloid progenitor cells. Survival of $CD45^+CD34^+CD33^+$ myeloid progenitors and $CD45^+CD34^-CD33^+$ precursors was assessed by annexin V binding assays and analyzed by FACS. Although the overall basal level of apoptosis is high in iPSC-derived myeloid progenitors for both control and SCN cells, the cells derived from *ELANE*-mutant SCN iPSCs show approximately 2-fold increased apoptosis in comparison to the control iPSC–derived myeloid progenitor cells (Supplemental Figure 7, A and B), suggesting enhanced apoptosis of *ELANE*-mutant SCN iPSC–derived myeloid progenitors. In agreement, the SCN iPSC–derived myeloid progenitors show approximately 2-fold reduced growth in myeloid expansion culture conditions (Supplemental Figure 7C).

We next analyzed the levels of apoptosis of myeloid precursor cells ($CD45^+CD34^-CD33^+$) differentiated from the iPSC-derived myeloid progenitors. After 5 days of culture in stem cell factor (SCF), IL-3, and GM-CSF (as outlined in Figure 1B), the myeloid progenitor cells lost CD34 expression and differentiated to myeloid precursors, mainly promyelocytes/myelocytes or monocyte precursors. We analyzed the apoptosis in these immature myeloid cells, as SCN iPSC–derived myeloid progenitor cells are arrested at this stage in their granulopoietic development. Similar to our findings in myeloid progenitors, the level of cell death is doubled in the *ELANE*-mutant SCN iPSC–derived myeloid precursor cells, indicating enhanced apoptosis compared with the control iPSC–derived myeloid precursor cells (Figure 2, A and B). We investigated the expression level of the BCL2 family of prosurvival and proapoptotic proteins in the promyelocytes derived from the control and *ELANE*-mutant SCN iPSCs. As shown in Figure 2C, the levels of *BCL2* mRNA are over 95% reduced in both the *ELANE*-mutant SCN iPSC–derived promyelocytes in comparison to control iPSC–derived cells. We also analyzed the expression level of BH3 domain only–containing BCL2 family proapoptotic proteins in these cells. The increased expression of BAX, BAD, and BIM, and the presence of cleaved forms of BIM, support the role of BH3-only proapoptotic molecules in the increased apoptosis in *ELANE*-mutant SCN iPSC–derived promyelocytes/myelocytes (Supplemental Figure 8A). To further examine the role of BCL2 in the survival of *ELANE*-mutant SCN iPSC–derived promyelocytes, we transduced the myeloid progenitor cells with a bicistronic retroviral construct expressing both murine Bcl2 and Thy1.1 through internal ribosomal entry site. Murine Bcl2 is highly homologous to human BCL2 and has been shown to retain the structural characteristics necessary to interface with pathways involved in the regulation of programmed cell death (27) while allowing mRNA quantitation of both endogenous and exogenous mRNA. The forced expression of Bcl2 increased approximately 2.5-fold the survival of granulocyte precursors, in comparison with vector-transduced cells, to levels similar to those found in control, mock-transduced precursor cells (Figure 2, D and F, and Supplemental Figure 8B). These data indicate that BCL2 plays a critical role in the apoptosis of *ELANE*-mutant SCN iPSC–derived myeloid precursor cells. Exogenous upregulation of the upstream BCL2 effector AKT was also explored through expression of constitutively active murine Akt (ca-*Akt*) in *ELANE*-mutant SCN iPSC–derived myeloid progenitors (Figure 2E). *ELANE*-mutant SCN iPSC–derived granulocyte precursors expressing ca-Akt had an approximately 2-fold increased survival (Figure 2F and Supplemental Figure 8B) and phenocopied the effect of *Bcl2* forced expression. These data indicate that, in addition to the differentiation arrest, the deficient survival of precursors is at the basis of the poor cell output of *ELANE*-mutant granulopoiesis.

Correction of ELANE mutations by CRISPR/Cas9 gene editing corrects differentiation arrest and survival of granulocytic precursors. To identify whether *ELANE* mutations were necessary to mediate SCN, we proceeded to repair SCN14 and SCN15 by genome editing. Two guide RNA sequences (RNA-seq) were selected to target the genome around *ELANE* exon 3 using clustered regularly interspaced short palindromic repeats (CRISPR) design tools (28). The 20-bp guide RNA sequences were cloned into the px330 chimeric SpCas9 and guide RNA vector. A targeting donor plasmid was constructed from a WT *ELANE* sequence that contained 800 bp 5′ and 1,500 bp 3′ homology arms from the CRISPR cut sites. For positive selection of donor integrants, a floxed cassette containing an *EFS* promoter driving EGFP was inserted between the homology arms (Supplemental Figure 9, A–C). The SCN iPSCs were transfected with the CRISPRs and donor plasmid; they were expanded, and GFP^+ cells were flow-sorted. GFP^+ colonies were then picked and expanded, and their mRNA was converted into cDNA and sequenced (Supplemental Figure 9, D and E) for verification of sequence of corrected *ELANE* expression. Quantification of overall mRNA expression of *ELANE* in promyelocytes derived from corrected isogenic lines showed similar levels of expression (Supplemental Figure 9F). The isogenic lines expressing corrected *ELANE* were identified as SCN14C and SCN15C — counterparts of SCN14 and SCN15, respectively.

To determine if gene correction of *ELANE* mutations restores graulopoietic differentiation, CRISPR-corrected SCN iPSCs were differentiated into $CD45^+CD34^+$ hematopoietic progenitors and then to terminally differentiated neutrophils using the methods described above. Both SCN14C and SCN15C generated similar levels of $CD45^+/CD34^+$ cells as their uncorrected parental counterparts, respectively (data not shown). When plated into semisolid methyl cellulose medium, $CD45^+CD34^+$ progenitors derived from CRISPR-corrected SCN iPSCs showed an increase of CFU-G over their corresponding noncorrected iPSC line (Figure 3A). Similarly,

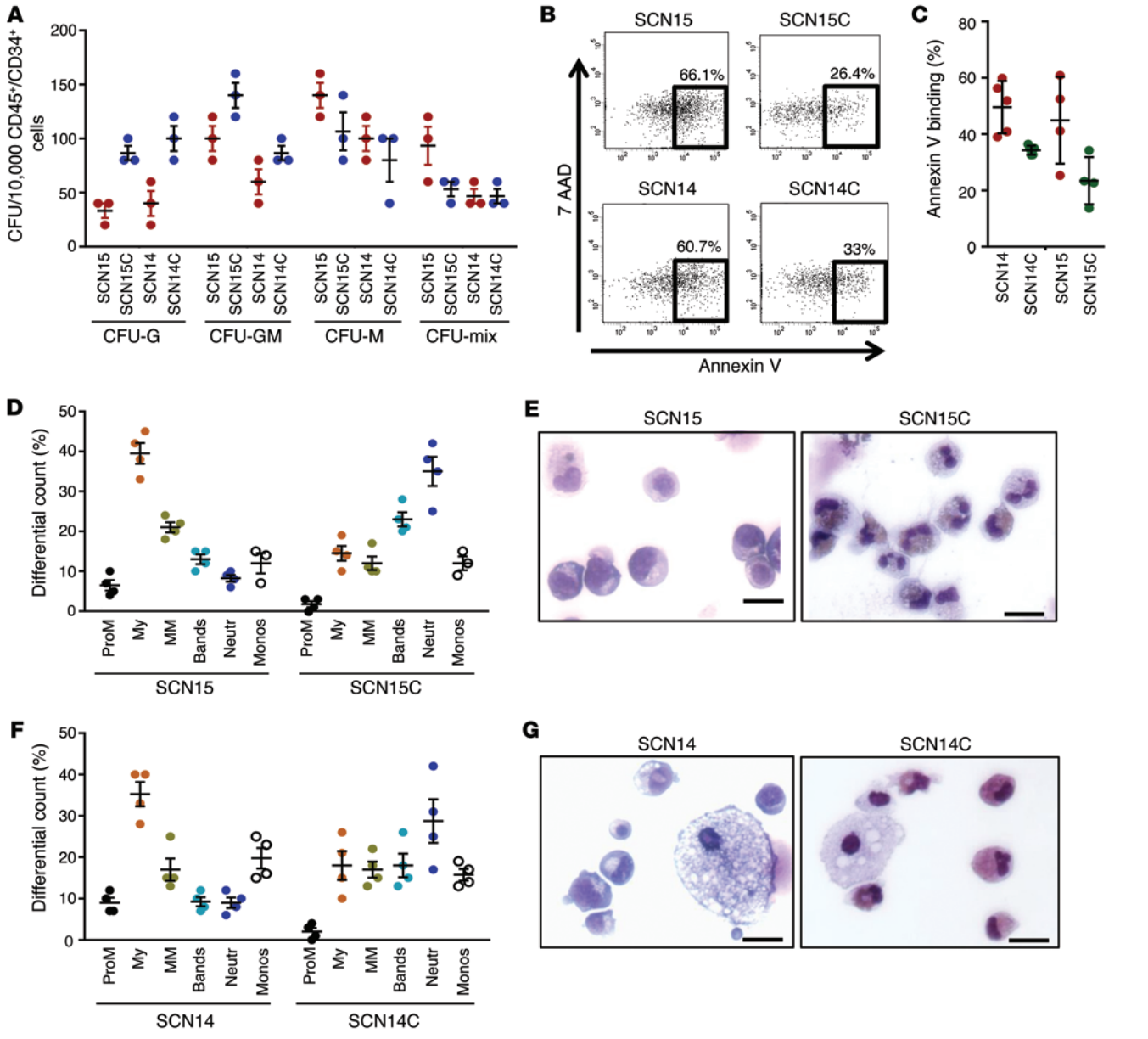

Figure 3. Cellular consequences of *ELANE* mutation: correction of *ELANE* mutation rescues granulocytic differentiation. (**A**) Colony forming cell assay of the hematopoietic progenitors derived from *ELANE*-mutant SCN iPSCs (SCN15, SCN14) and the derivative *ELANE* mutation–corrected iPSCs (SCN15C, SCN14C). (**B**) Representative example of annexin V binding analysis in *ELANE* mutant– and CRISPR-corrected iPSC–derived granulocytic precursors. (**C**) Quantitation of the % annexin V binding. (**D**) Quantitation of granulopoietic differentiation of myeloid progenitors derived from SCN iPSCs (SCN15) and the corrected iPSCs (SCN15C). (**E**) Wright-Giemsa–stained cytospin at the end of the culture (SCN15, SCN15C). (**F**) Quantitation of granulopoietic differentiation of myeloid progenitors derived from SCN iPSCs (SCN14) and the corrected iPSCs (SCN14C). (**G**) Wright-Giemsa–stained cytospin at the end of the culture (SCN14, SCN14C). Data are presented as mean ± SD of 3 or 4 independent experiments.

corrected expression of NE results in improved survival (Figure 3, B and C) and granulocytic differentiation (Figure 3, D–G). These data resolve the critical role for these *ELANE* point mutations in the development of SCN-like disease.

ELANE-mutant SCN iPSC–derived myeloid precursor cells contain mislocalized NE. We interrogated our iPSC models to understand the possible pathobiological mechanisms of disease and to identify targets for intervention. Two hypotheses on how *ELANE* mutations affect NE have been proposed. In one, mutant NE is mistrafficked, while, in the other, mutant NE misfolds, resulting in activation of the UPR in the ER (16, 17, 29). We have previously demonstrated that alternative start codons in *ELANE* result in the translation of multiple peptides, which are susceptible to overwhelm the UPR system and induce ER stress, and in reduced clonogenic capacity of myeloid lineage cells (22). We analyzed the expression level of UPR pathway genes, and similar to the reports in primary cells, we found an approximately 2-fold increase of mRNA levels of the UPR pathway genes *BIP* and *ATF6* in the *ELANE*-mutant SCN iPSC–derived promyelocytes, compared with control iPSC–derived cells (Figure 4A), which were not cor-

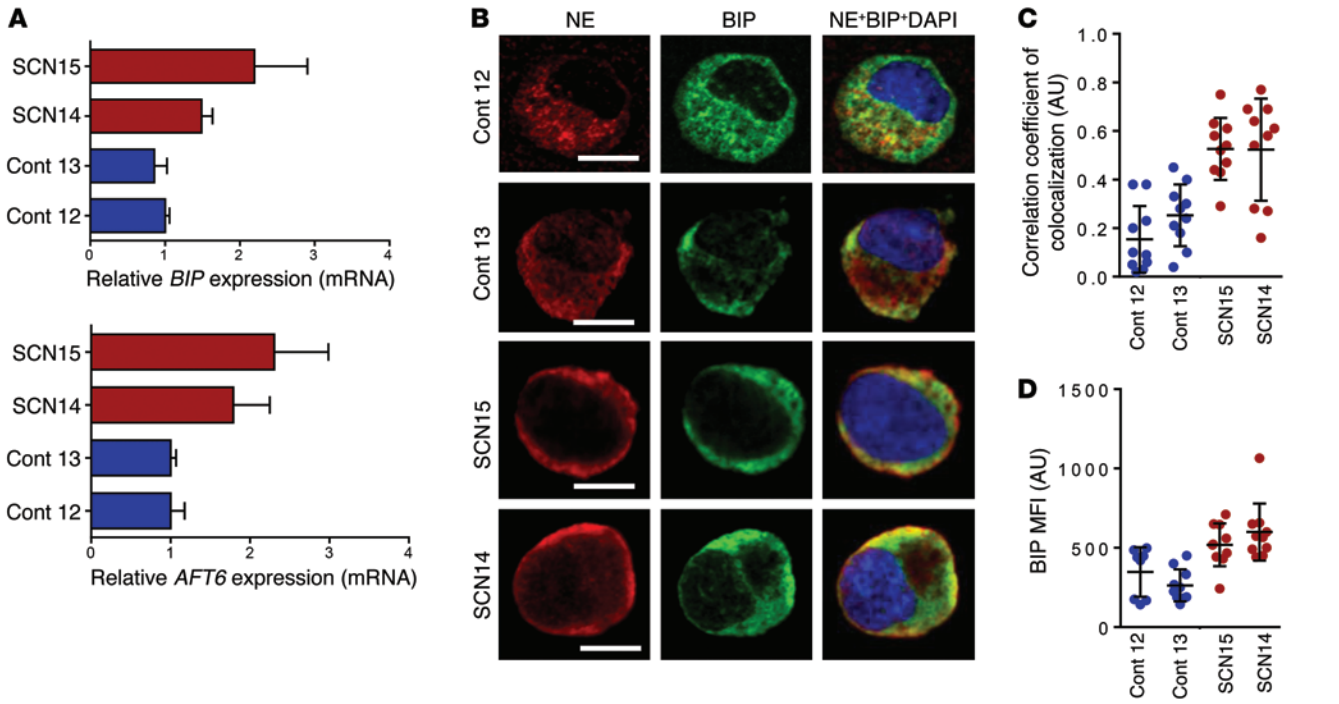

Figure 4. ER stress and NE mislocalization are hallmarks of *ELANE*-mutant iPSC–derived granulocytic precursors. (**A**) qPCR analyses of the mRNA for UPR pathway genes *BIP* and *ATF6* in RNA from control and SCN iPSC–derived promyelocytes. (**B**) Confocal microscopic analyses of the localization of NE and ER resident chaperone BIP in control and SCN iPSC–derived promyelocytes. Scale bars: 10 μm. (**C**) Quantitation of the correlation of colocalization coefficient between NE and BIP. (**D**) MFI of BIP measured from confocal microscopic images. In **A**, individual values of 2 or more independent experiments in duplicate are plotted as mean ± SD. In **C** and **D**, data from more than 10 cells from 2 independent experiments are presented as mean ± SD. Cont, control.

rected by downstream prosurvival signals from forced expression of Bcl2 and ca-Akt (Supplemental Figure 10, A and B). This effect happened despite similar levels of expression of NE at mRNA and protein levels, and similar NE proteolytic activity in control and *ELANE*-mutant SCN iPSC–derived promyelocytes (Supplemental Figure 10, C–E). Analysis of the cellular distribution in the subcellular compartments of promyelocytes/myelocytes unveiled a punctate and granular distribution of NE in control iPSC–derived promyelocytes/myelocytes. In contrast, the NE was predominantly localized beneath the plasma membrane in *ELANE*-mutant SCN iPSC–derived promyelocytes/myelocytes (Figure 4B). NE was colocalized with BIP in both control and *ELANE*-mutant SCN iPSC–derived promyelocytes, but there was an approximately 2.5-fold increase in the colocalization coefficient between NE and BIP in *ELANE*-mutant SCN iPSC–derived promyelocytes (Figure 4C), suggestive of improper trafficking of the protein from the ER. The elevated level of BIP mean fluorescence intensity (MFI) (Figure 4D) and the colocalization with NE may support a role of ER stress–induced UPR. These data suggest that the 2 aforementioned mechanisms of neutropenia may represent a common phenomenon contributing to SCN pathobiology: the mislocalization of mutant NE, which induces UPR/ER stress.

High dose of G-CSF or lower G-CSF combined with NE inhibition rescues neutrophil maturation. In most cases, mutant-*ELANE* SCN patients show a partial response to extremely high doses of G-CSF with an increase in neutrophil count in the PB and reduction of the frequency and severity of bacterial and fungal infections (4). However, frequent administration of high doses of G-CSF does not correct abnormal neutrophil function (3) and has been argued to lead to the development of myelodysplastic syndrome/acute myelogenous leukemia in more than 25% of the treated patients (4, 30). To examine the effect of high doses of G-CSF in the granulocytic maturation of *ELANE*-mutant SCN iPSC–derived myeloid progenitors, we added G-CSF to the culture at 1,000 ng/ml during the last 5 days of granulocytic differentiation (as depicted in Figure 1B). As shown in Figure 5, A and C, the granulocytic maturation of myeloid progenitors derived from both *ELANE*-mutant SCN iPSC lines cultured in the presence of a high concentration of G-CSF was rescued with an increase in the neutrophil output and a concomitant decrease in the promyelocytic and myelocytic populations, compared with the granulopoiesis in lower concentrations (50 ng/ml) of G-CSF. Cytospin analysis (shown in Figure 5, B and D) shows mature granulocytes from cultures containing 1,000 ng/ml G-CSF and only shows immature granulocytic cells when myeloid progenitors are cultured in 50 ng/ml G-CSF. The *ELANE*-mutant SCN iPSC–derived promyelocytes expressed similar levels of NE, retained protease activity, and accumulated in the ER lumen and other cytosolic regions outside the primary granules. We hypothesize that the inhibition of NE activity may ameliorate cell damage associated with mislocalized NE in *ELANE*-mutant SCN iPSC–derived myeloid precursor cells. Sivelestat (also called ONO-5046) is an NE-specific cell-permeant serine protease inhibitor used in the treatment of acute lung injury. We added sivelestat with G-CSF during the final 5 days of granulopoietic differentiation culture. Differential counts revealed that neutrophil differentiation of *ELANE*-mutant SCN iPSC–derived myeloid pre-

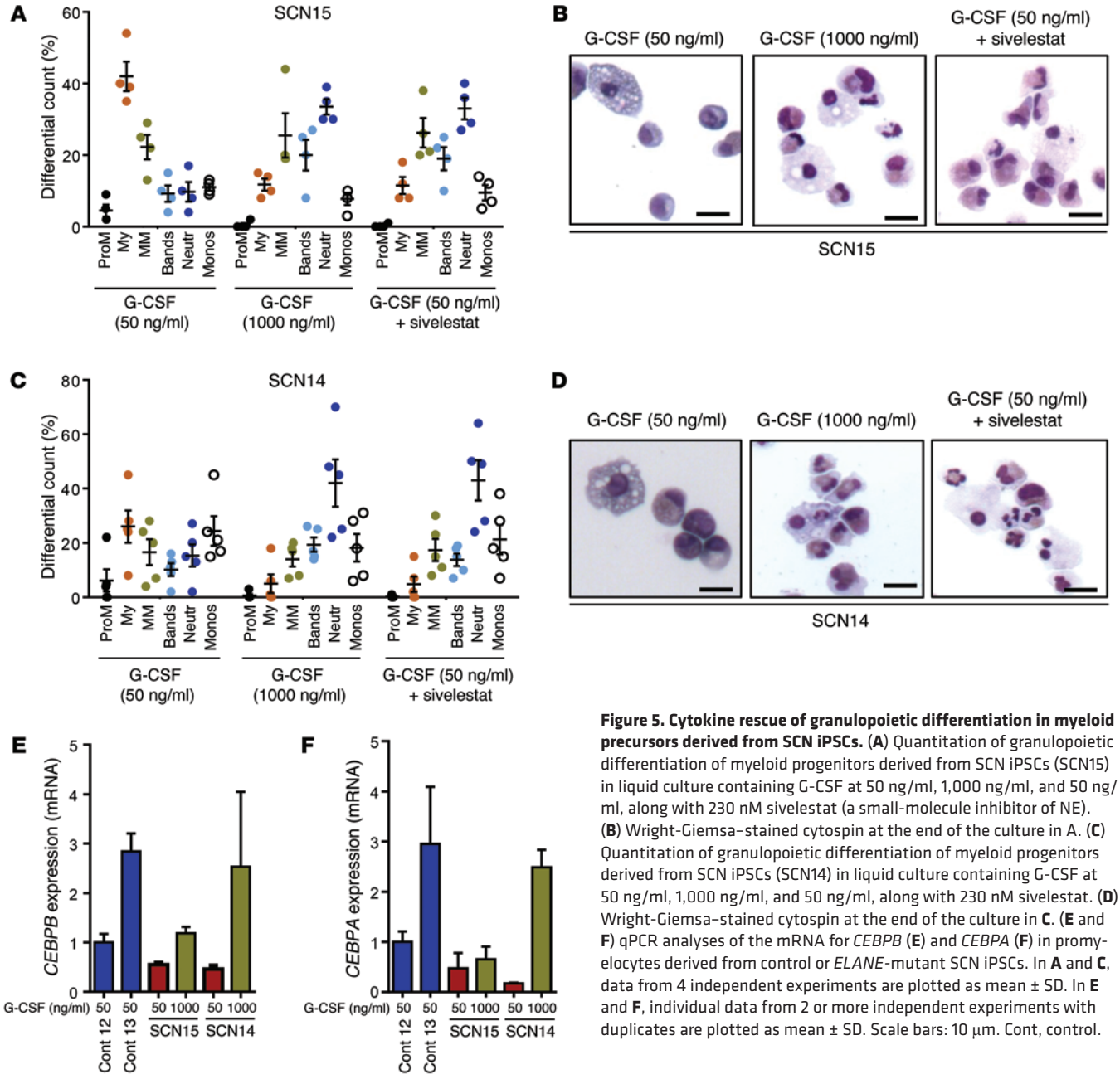

Figure 5. Cytokine rescue of granulopoietic differentiation in myeloid precursors derived from SCN iPSCs. (**A**) Quantitation of granulopoietic differentiation of myeloid progenitors derived from SCN iPSCs (SCN15) in liquid culture containing G-CSF at 50 ng/ml, 1,000 ng/ml, and 50 ng/ml, along with 230 nM sivelestat (a small-molecule inhibitor of NE). (**B**) Wright-Giemsa–stained cytospin at the end of the culture in A. (**C**) Quantitation of granulopoietic differentiation of myeloid progenitors derived from SCN iPSCs (SCN14) in liquid culture containing G-CSF at 50 ng/ml, 1,000 ng/ml, and 50 ng/ml, along with 230 nM sivelestat. (**D**) Wright-Giemsa–stained cytospin at the end of the culture in **C**. (**E** and **F**) qPCR analyses of the mRNA for *CEBPB* (**E**) and *CEBPA* (**F**) in promyelocytes derived from control or *ELANE*-mutant SCN iPSCs. In **A** and **C**, data from 4 independent experiments are plotted as mean ± SD. In **E** and **F**, individual data from 2 or more independent experiments with duplicates are plotted as mean ± SD. Scale bars: 10 μm. Cont, control.

cursor cells was markedly increased and the frequency of immature myeloid cells (promyelocytes and myelocytes) was drastically decreased in the presence of 50 ng/ml G-CSF in combination with sivelestat (Figure 5, A–D). Further, the SCN iPSC–derived cultures with sivelestat also contained mature neutrophils and monocytes, indicating that the block in neutrophil differentiation was eliminated in the presence of sivelestat.

CCAAT/enhancer-binding protein alpha (C/EBPα) and its isoform C/EBPβ are crucial regulators of basal and emergent granulopoiesis, respectively (31, 32). We analyzed the expression levels of these 2 transcription factors to unravel the cellular mechanism behind sivelestat-mediated rescue and to determine whether sivelestat and high-dose G-CSF act through common or different mechanisms. Previous reports suggested that mutations in *ELANE* result in significant reduction in the expression levels of both *CEBPA* and *CEBPB* (33), as well as LEF1, a putative transcriptional regulator of *CEBPA* downstream of Wnt/β-catenin signaling (11, 34). Our data from SCN iPSC–derived granulopoiesis confirmed that the expression of these factors is low (Figure 5, E and F, and Supplemental Figure 11), but we note that the expression of the *CEBPA* and *CEBPB* was corrected in genome-edited iPSC–derived granulocytic precursors (Supplemental Figure 12, A and B). The addition of a high dose of G-CSF to *ELANE*-mutant iPSC–derived myelopoiesis results in the consistent upregulation of C/EBPβ, along with upregulation of C/EBPα expression, to control levels in granulocytic precursors generated from the SCN14 line but not from the SCN15 line (Figure 5, E and F). Interestingly, the addition of sivelestat to granulopoietic cultures restored

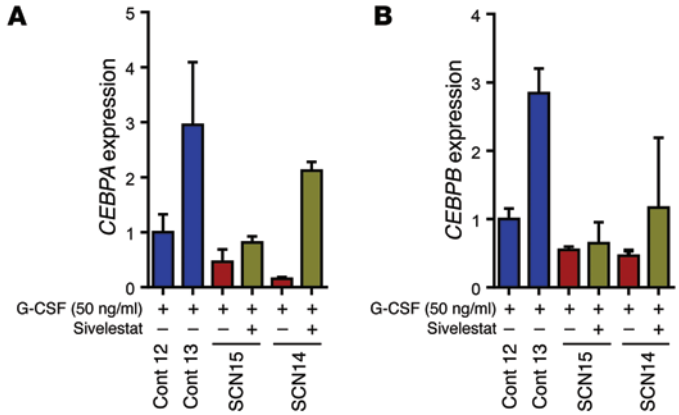

Figure 6. Sivelestat rescue of SCN iPSC neutrophil maturation is associated with correction of *CEBPA*, but not *CEBPB*, expression and NE mislocalization. (**A** and **B**) qPCR assay in sorted promyelocytes/myelocytes. (**A**) Relative expression of *CEBPA*. (**B**) Relative expression of *CEBPB*. (**C**) Confocal microscopic localization of primary neutrophil granule proteins NE and MPO in control and SCN iPSCs, and exon 3 mutation–corrected iPSC–derived (SCN15C-derived) promyelocytes. Arrow indicates the colocalization of NE and MPO in primary granules. Scale bars, 10 μm. (**D**) Quantitation of the correlation of colocalization coefficient between NE and MPO in the primary granules in **C**. (**E**) MFI of NE at MPO marked primary granules. In **A** and **B**, individual data from 2 or more independent experiments in duplicate are plotted as mean ± SD. In **D** and **E**, values of 8 or more cells from 2 independent experiments are presented as mean ± SD. Cont, control.

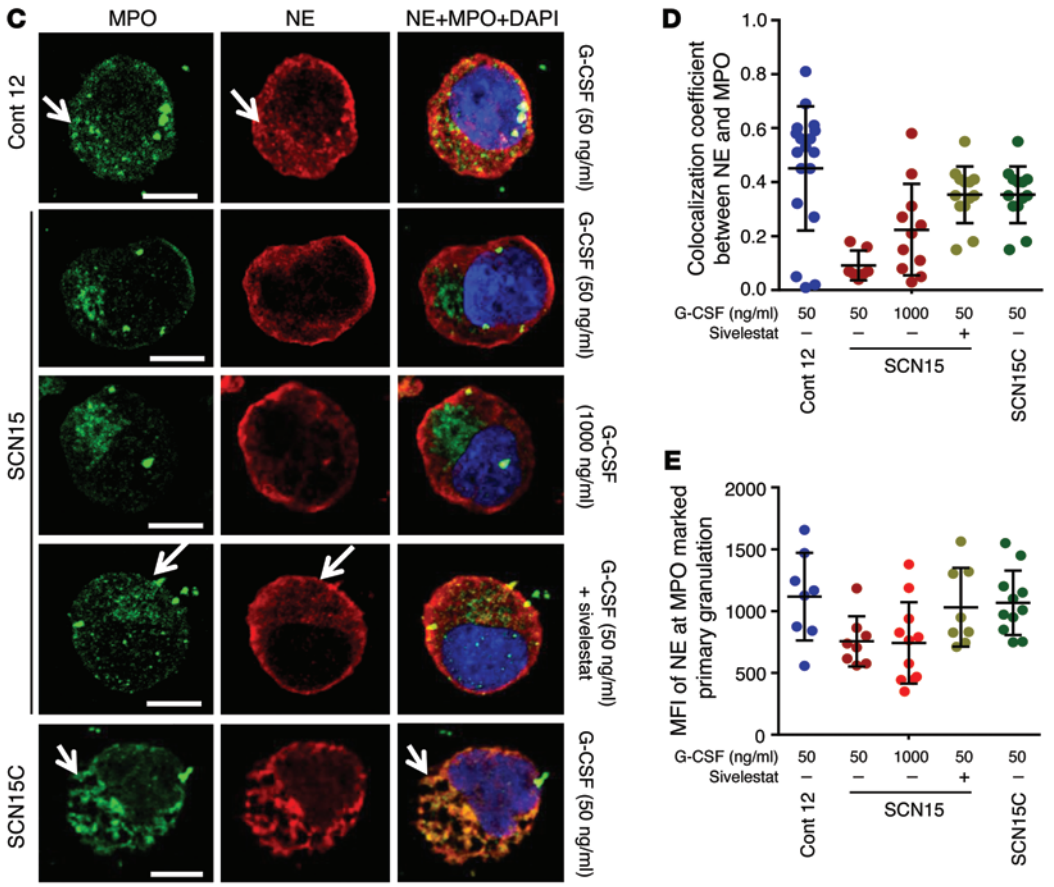

expression of *CEBPA*, which regulates basal granulopoiesis, but did not induce *CEBPB* expression, which regulates emergency granulopoiesis (Figure 6, A and B). Neither treatment modified the levels of *CEBPA* or *CEBPB* in normal iPSC–derived promyelocytes (Supplemental Figure 12, C and D). These results suggest that this pharmacological approach may distinctly rescue basal granulopoiesis in the context of mutant *ELANE*.

To further delineate the mechanism behind the amelioration of ER stress and the upregulation of prosurvival gene expression, we investigated the cellular localization of NE in the presence of sivelestat. At the promyelocyte stage, NE traffics from the ER lumen and is primarily distributed in the primary granules of promyelocytes and more differentiated granulocytic precursors and neutrophils (35, 36). Normally, NE is synthesized as a transient proform that becomes catalytically active by removal of an N-terminal propeptide after granule targeting (37). Mislocalization of activated mutant NE has been argued to be pathogenetically implicated in SCN in vitro and in vivo (14, 17, 38). To determine whether sivelestat may also modify the mislocalization of NE, we analyzed the colocalization of NE with myeloperoxidase (MPO), a bona fide primary granule marker, in the promyelocytes/myelocytes derived from control and *ELANE*-mutant SCN iPSCs. NE and MPO colocalized in punctate and granular patterns (Figure 6, C–E, and Supplemental Figure 13, A–C) — coinciding in form and shape with the pattern of expression of primary granules — in control iPSC–derived promyelocytes/myelocytes (39). However, NE

and MPO in *ELANE*-mutant iPSC–derived promyelocytes/myelocytes presented a completely different pattern, with abundant NE located outside the primary granules, in subcortical regions without colocalization with MPO. Mislocalization of NE was not modified by the concentration of G-CSF, as no difference was found between promyelocytes/myelocytes from cultures containing 50 ng/ml or 1,000 ng/ml G-CSF (Figure 6, C–E). Interestingly, the mislocalization of NE is reversed by the addition of sivelestat at levels similar to those reached by the genetic correction of *ELANE* expression to cultures containing 50 ng/ml of G-CSF (Figure 6, C–E, and Supplemental Figure 13, A–C). The addition of sivelestat induced an approximately 3-fold increase in the correlation coefficients of colocalization between NE and MPO in the primary granules of *ELANE*-mutant–derived promyelocytes at levels similar to those reached by the genetic correction of *ELANE* expression (Figure 6, C–E, and Supplemental Figure 13, A–C). Furthermore, the addition of sivelestat markedly reduced the mRNA expression level of ER stress–induced UPR pathway genes *BIP* and *ATF6,* and of BIP protein expression in promyelocytes/myelocytes derived from *ELANE*-mutant iPSCs (Supplemental Figure 13, D–F) at levels similar to those reached by the genetic correction of *ELANE* expression (Supplemental Figure 13, G–H). At the same time, sivelestat also increased the survival and, modestly, the cell expansion of SCN iPSC–derived postmitotic granulocytic precursors (Supplemental Figure 14, A–C) and the expression level of the prosurvival gene *BCL2* in the *ELANE*-mutant iPSC–derived promyelocytes (Supplemental Figure 14D) at levels similar to those reached by the genetic correction of *ELANE* expression (Supplemental Figure 14E), indicating that sivelestat ameliorates the ER stress and enhances cellular survival. These results indicate that sivelestat corrects the mislocalization of NE, ameliorates ER stress, reduces the UPR, and upregulates the expression level of *CEPBA* and *BCL2* and the survival of *ELANE* mutant granulocyte precursors.

Discussion

Animal models and in vitro cultures consisting of cells derived from patients are often used to investigate disease pathophysiology and to develop therapies. Unfortunately, mutant-*ELANE* knockin mice fail to reproduce the abnormal granulopoiesis, as observed in SCN patients (18, 19). Moreover, BM cells are not an ideal experimental tool, since it is difficult to obtain sufficient nucleated cells due to the invasiveness of the aspiration procedure in pediatric patients with rare BM-failure syndromes. Moreover, the analysis of pathobiological mechanisms occurring during different stages of granulopoietic differentiation is difficult to address in primary patient samples where most of myelopoiesis is already arrested in the promyelocyte stage.

iPSCs have been shown to be an excellent tool to analyze pathogenetic mechanisms and for drug discovery (40–42). The use of iPSCs to address mechanisms of disease in SCN has been documented by our group and other groups (21, 22, 43). In this report, we first demonstrate that SCN-associated single point mutations in one allele of *ELANE* are necessary to induce granulopoietic differentiation arrest and apoptosis of granulocytic progenitors and precursors. This model confirms some of the current concepts of pathogenesis induced by heterozygote mutations of *ELANE*. First, the correction of *ELANE* mutations corrects granulopoietic defects and progenitor differentiation biases in iPSC-derived myelopoiesis, indicating that the mutations in one allele of *ELANE* are crucial contributors to the development of the key pathobiological features of this disease. Of course, other modifier genes may ameliorate or worsen the pathobiological features of mutant-*ELANE* SCN. Second, the deficient survival of granulocytic precursors derived from mutant-*ELANE* iPSCs depends on functional G-CSF signaling and can be rescued by restoration of deficient downstream Akt/Bcl2 signaling, a common feature in apoptosis induced by ER stress (44, 45). This finding provides crucial information on the mechanisms controlling survival of diseased granulocytes. Notably, overexpression of activated Akt and downstream Bcl2 cannot increase the lifespan of normal granulocytes (46), but it does in other pathological situations, like sepsis (47). Third, high doses of G-CSF result in the amelioration of dysgranulopoiesis, granulocyte precursor survival defects, as previously shown in iPSC-derived granulopoiesis (21), and of *CEBPB* expression levels, as shown in primary myelopoiesis from patients (11, 48). Notably, our data cannot rule out the existence of genes that modify the clinical and biological features of ELANE mutations that would affect the severity of the disease; for instance, such mutations could induce SCN in some patients and cyclic neutropenia in others (6).

NE is a glycoprotein with a single peptide chain of 218 amino acid residues and 4 disulfide bridges. Mutant NE–expressing granulocytic precursors show aberrant expression of NE outside primary granulation, with accumulation in the ER and subcortical intracellular spaces. NE mistrafficking correlates with the accumulation of NE in the ER, which induces stress that can be corrected by the addition of the NE inhibitor sivelestat to cultures of iPSC-derived myelopoiesis. Sivelestat activity is facilitated by a catalytic triad conserved in all serine proteases that consists of His 57, Asp102, and Ser195 residues forming a charge relay system. In NE, the S1 pocket containing the primary sivelestat binding domain is specifically modified, is rather hydrophobic, and has a hemispheric shape, causing the sivelestat to dock to NE with a higher affinity than most other serine proteases (49). Neither of the 2 mutations analyzed in this study affect the catalytic site, and therefore, the NE activity is unaffected and similar to controls (as shown in Supplemental Figure 10). Changes in the S1 pocket structure, as induced by sivelestat (49), may result in increased proton relaxation of residues that are crucial for tertiary structure folding of NE and alternatively translated proteins (22). Our data demonstrate that both mutations of *ELANE* result in intracellular mistrafficking of NE and/or alternatively translated proteins, which conserve the C-terminus region recognized by the anti-NE antibody used in our microscopy and immunoblot experiments. In our studies, sivelestat correction of impaired intracellular traffic of NE in *ELANE*-mutant granulocytic precursors restored *CEBPA* expression, granulopoietic differentiation, and granulocytic survival at levels similar to those reached by the isogenic correction of the *ELANE* mutation and, unlike high-dose G-CSF, failed to use the *CEBPB* expression–associated pathway of emergent granulopoiesis. These data suggest that, in addition to its inhibitory activity, the binding of sivelestat to NE induces conformational changes that prevent its mislocalization and ameliorate ER stress, resulting in restoration of granulocytic precur-

sor survival, granulocyte differentiation, and *CEBPA* expression. While the precise mechanism of sivelestat remains unknown, it can be postulated that the high-binding affinity of sivelestat for NE (reviewed in ref. 50) may result in acting as a pharmacological chaperone with activity on protein folding and proteostasis (51, 52). In any event, the cellular mechanism used by sivelestat is different from the one employed by high-dose G-CSF. Namely, while high-dose G-CSF induces emergency granulopoiesis through upregulation of C/EBPβ, sivelestat acts directly through the normal granulocytic differentiation pathway, as evidenced by normalization of C/EBPα expression levels. Thus, we propose that SCN disease pathogenesis pivots upon NE mislocalization, which triggers UPR/ER stress and dysfunctional differentiation and survival signaling. Our work provides a paradigm that can be clinically exploited to achieve therapeutic responses by using lower doses of G-CSF in combination with small-molecule targeting to correct NE mislocalization, easing the management of these patients and possibly impacting the probability of these patients to develop clonal evolution and malignant disease.

Methods

Origin of cellular material used for analysis. No clonal cell lines were generated. All the lines used were expected to be polyclonal or, at the very minimum, oligoclonal. One line was generated from each of 2 healthy donors ($n = 2$) and from each of 2 patients with heterozygote point mutations in exon 3 of *ELANE* ($n = 2$) for the experiments described in the study. One noncloned, isogenic CRISPR/Cas9-corrected line was produced per patient-derived parental iPSC line by bulk FACS sorting of EGFP$^+$ cells where EGFP expression was used as a reporter of corrected ELANE exon 3 (Supplemental Figure 9C). A total of 6 lines were studied in this report. No specific selection of clones was used during the process.

Generation of iPSCs from healthy donor and ELANE-mutant SCN patient PB MNCs. PB from healthy donors and SCN patients was obtained at Cincinnati Children's Hospital Medical Center through informed consent under an approved institutional review board research protocol. iPSCs were generated from PB MNCs as described (53). Briefly, PB MNCs were purified from PB by Ficoll separation (GE Healthcare) and plated at 5×10^6 cells/ml in X-VIVO 10 (Lonza) supplemented with 10% FCS, SCF (100 ng/ml), TPO (100 ng/ml), IL-3 (100 ng/ml), IL-6 (20 ng/ml), FLT3L (100 ng/ml), and GM-CSF (10 ng/ml) (all cytokines from PeproTech) in a low-attachment plate (Corning) and cultured at 37°C in 5% CO_2. After 2 days of culture, cells were transduced with a lentivirus containing OCT4, KLF4, MYC, and SOX2 (54) using polybrene at a MOI of 20–40. Two days after lentiviral transduction, cells were plated onto irradiated mouse embryonic fibroblasts (MEF, GlobalStem) in X-VIVO 10 supplemented with 10% FCS, SCF (100 ng/ml), TPO (100 ng/ml), IL-3 (10 ng/ml), IL-6 (20 ng/ml), and FLT3L (100 ng/ml). After 2 days of culture on MEF, the media was changed to hESC media (DMEM F/12, 20% KnockOut Serum Replacement (KSR, Invitrogen), 1% L-glutamine, 1% NEAA, 0.1 mM β-mercaptoethanol) supplemented with 10 ng/ml bFGF (PeproTech), and a small-molecule iPSC enhancement cocktail containing SB431542 (2 μM, Miltenyi Biotec), PD0325901 (0.5 μM, Cayman Chemical), and Thiazovivin (2 μM, Stemgent). After 10 days, the small molecules were removed and the medium was changed every other day. Once iPS-like colonies were observed, they were plucked and passaged onto fresh MEF and cultured with hESC media or onto Matrigel (BD Biosciences) and cultured in mTeSR1 medium (StemCell Technologies Inc.).

Hematopoietic differentiation of healthy donor– and SCN patient–derived iPSCs and FACS characterization. Hematopoietic differentiation was carried out as described (23) with minor modifications. Briefly, 5×10^5 cells were plated on growth factor–reduced Matrigel (BD Biosciences) and cultured for 24 hours in hES media supplemented with 10 mM ROCK inhibitor Y-27632 (Millipore). After 24 hours, media was changed to RPMI supplemented with L-glutamine, ascorbic acid (50 μg/ml), monothioglycerol (100 μM), BMP4 (5 ng/ml), CHIR99021 (930 ng/ml), and VEGF (50 ng/ml). Twenty-four hours after media change, CHIR99021 was removed from the culture medium and bFGF was added at 20 ng/ml. On day 3, medium was changed to StemPro 34 (Invitrogen) containing BMP4 (5 ng/ml), bFGF (20 ng/ml), and VEGF (50 ng/ml). On days 4–5, cells were cultured in StemPro34 containing VEGF (15 ng/ml) and bFGF (5 ng/ml). On day 6, media was changed to serum-free SFD media with VEGF (50 ng/ml), Flt3L (5 ng/ml), SCF (50 ng/ml), and bFGF (50 ng/ml). For days 7–10, cells were cultured in SFD with VEGF (50 ng/ml), Flt3L (5 ng/ml), SCF (50 ng/ml), TPO (50 ng/ml), and IL-6 (10 ng/ml). Nonadherent cells were collected from the media on days 8–10; stained with the antibodies (all from BD Biosciences) for CD45-PacificBlue (catalog 560367, clone HI30), CD34-PECy7 (catalog 560710, clone 581), CD33-APC (catalog 551378, clone WM-53), and CD43-FITC (catalog 555475, clone 1G10); and FACS analyzed.

CFU assays. Progenitor content and activity were evaluated in CFU assays using standard conditions. In brief, 2,500 nonadherent cells were mixed in 1 ml of methyl cellulose semisolid medium containing cytokine mixture (MethoCult H4034 Optimum, StemCell Technologies), and seeded into a 35-mm gridded disc. The disc containing cells in methyl cellulose semisolid medium was incubated at 37°C in a humidified 5% CO_2 incubator. The hematopoietic colonies (CFU-G, CFU-M, CFU-GM, and CFU-Mix) generated were scored at day 14 under an inverted microscope. In order to quantify the number of hematopoietic progenitors at the time of plating, an aliquot of the nonadherent cells from control and SCN iPSCs on day 10 of hematopoietic differentiation was analyzed for CD45$^+$ and CD34$^+$ expression by flow cytometry. The number of colonies was normalized per 10,000 CD45$^+$CD34$^+$ by multiplying the percentage of CD45$^+$/CD34$^+$ cells in the initiating cell population derived from each sample by the number of each colony type.

Myeloid cell expansion and granulopoiesis of iPSC-derived hematopoietic progenitors. iPSCs were differentiated into hematopoietic progenitors by 10 days of culture in myeloid expansion medium (IMDM + Ham's F12 at 3:1 ratio) containing 0.5% N2 supplement, 1% B27 supplement without vitamin A, 0.5% human serum albumin, 100 μM monothioglycerol, 50 μg/ml ascorbic acid, 100 ng/ml recombinant SCF, 10 ng/ml IL-3, and 10 ng/ml GM-CSF. The cultures were further differentiated using granulopoietic culture conditions (IMDM + Ham's F12 at 3:1 ratio) containing 0.5% N2 supplement, 1% B27 supplement without vitamin A, 0.5% human serum albumin, 100 μM monothioglycerol, 50 μg/ml ascorbic acid, and 50 ng/ml G-CSF (Neupogen filgrastim) for 5 days. At the granulopoietic differentiation stage, cells were cultured at low (50 ng/ml) or high (1,000 ng/ml) G-CSF doses. During myeloid expansion and granulopoietic differentiation, cells were cultured in presence or absence of Sivelestat (Sigma-Aldrich) at a concentration of 230 nM (~5 times the IC50

for NE) (55). At the end of granulopoietic differentiation, cells were cytospun onto a Superfrost Plus Microscope slide (Fisher Scientific). The cells were Wright-Giemsa stained and then scored for myeloid cell types (promyelocytes, myelocytes, metamyelocytes, bands, neutrophils, and monocytes) using an upright microscope (Motic BA310). For sorting of the promyelocytes, cells at the end of myeloid expansion were stained for CD45-Pacific Blue, CD34-PECy7, CD33-APC, CD11b-APCCy7 (catalog 557754, clone ICRF44, BD Biosciences), and CD15-FITC (catalog 562370, clone W6D3, BD Biosciences). The promyelocytes/myelocyte population (defined as $CD45^+/CD34^-/CD33^+/CD11b^-/CD15^{dim}$) was selected by FACS.

Isolation and transcriptome analysis of myeloid populations isolated from BM- or iPSC-derived cultures. Hematopoietic progenitors derived from control and SCN iPSCs were cultured in myeloid expansion medium containing 50 ng/ml SCF, 10 ng/ml IL-3, and 10 ng/ml GM-CSF for 5 days. The cells at this point were stained for CD45-Pacific blue, CD34-PECy7, CD33-APC, CD11b-APC-Cy7, and CD15-FITC. 7-AAD was used to eliminate the dead cells. The promyelocytic population ($CD45^+CD34^-CD33^+CD11b^-CD15^{+/lo}$) was sorted, and the RNA from control and SCN iPSC promyelocytes was isolated using QIAGEN RNeasy Mini Kit. Transcriptional comparisons with healthy subject–derived iPSC lines (n = 7), mesoderm (first 7 days of the differentiation protocol, as published elsewhere, from 4 healthy subject–derived iPSC lines, n = 4; ref. 24), sorted BM and iPSC-derived myeloid progenitors ($CD45^+CD34^+CD45RA^+$ or $CD45^+CD34^+CD33^+$, respectively, n = 2–3 per group), BM promyelocytes (n = 2), and control iPSC–derived promyelocytes (n = 2) were performed. Total RNA was extracted from sorted populations derived from BM or iPSCs using RNeasy Mini Kit (QIAGEN) or TRIzol (Invitrogen) as required for the number of cells available. RNA quality and concentration were measured by Bioanalyzer 2100 using the RNA 6000 Nano Assay (Agilent Technologies). For RNA specimens obtained from fewer than 50,000 cells (sorted BM populations and iPSC-derived promyelocytes and progenitors), a linear amplification sequencing protocol was performed (Illumina). RNA-seq libraries were prepared using the Illumina TruSeq RNA preparation kit and sequenced on the Illumina HiSeq 2000 using single-end 20 million–bp reads. Reads were aligned with TopHat software, using hg19 as the reference genome and mapping reads per kilobase per million mapped reads (RPKM) as output. RPKM were log2-transformed and base-lined to the median expression of the average of each class of samples (iPSC-derived myeloid progenitors, BM progenitor/promyelocytes, iPSCs, and iPSCs differentiated to mesoderm). Differentially expressed genes were identified from a starting pool of all transcripts with more than 3 fragments per kilobase of exon per million fragments mapped (FPKM) in at least 2 of the 9 myeloid samples (12,859 gene-level summarized transcripts). For all these populations, the RNA samples were processed for RNA-seq analyses using RNA-seq protocol from NuGEN and Illumina. The amplified products were sequenced to analyze the gene expression profile. All original microarray data were deposited in the NCBI's Gene Expression Omnibus (GEO GSE69622).

Retroviral transduction of hematopoietic progenitor cells. Hematopoietic progenitors ($CD45^+$ $CD34^+$) derived from control or SCN iPSCs at day 10 of hematopoietic differentiation were collected and cultured in myeloid expansion medium containing 100 ng/ml recombinant SCF, 10 ng/ml IL-3, and 10 ng/ml GM-CSF for 12 hours, on Retronectin-coated (CH-296, Takara Bio Inc.) nontissue culture dishes. Recombinant retroviral vector supernatant carrying ca-Akt, murine Bcl2, or empty vector control were added for 8-hour transduction. At the end of transduction, cells were washed and cultured in myeloid expansion medium containing 100 ng/ml recombinant SCF, 10 ng/ml IL-3, and 10 ng/ml GM-CSF for 4 days. Myeloid precursor cells were analyzed for apoptosis using an annexin V staining kit according to the manufacturer's instructions (BD Pharmingen). Early apoptosis was determined as annexin V–positive events on $CD45^+$ hematopoietic cells after gating out large residual dead ($7\text{-}AAD^+$) iPSCs. Cells expressing CD90.1 were gated and analyzed, as the retroviruses express CD90.1 through internal ribosomal entry site (IRES). Ninety-six hours after transduction, cells expressing CD90.1 were sorted and cultured in granulocyte differentiation medium containing 50 ng/ml G-CSF (Neupogen filgrastim) for 5 days for the cytospin analyses of myeloid differentiated cells.

Quantitative PCR. Total RNA was extracted from the promyelocytes derived from control SCN iPSCs, or SCN mutation–corrected iPSCs using RNeasy minikit (QIAGEN) following the manufacturer's instructions, and cDNA was prepared using TaqMan reverse transcription reagent (Roche Applied Science). The mRNA expression levels of Bcl2, BIP, ATF6, ca-Akt, CEBPA, and CEBPB were analyzed by quantitative PCR (qPCR) assay using TaqMan Universal PCR master mix and TaqMan primers for specific genes (Roche Applied Science). The expression level was normalized with the expression of internal control gene GAPDH.

Western blot analyses. Hematopoietic progenitors derived from control or SCN iPSCs were cultured in myeloid expansion medium containing 100 ng/ml recombinant SCF, 10 ng/ml IL-3, and 10 ng/ml GM-CSF for 5 days. Promyelocytes from these cultures were sorted, and protein samples were prepared by lysing them in 1× RIPA buffer containing protease inhibitor cocktail and phosphatase inhibitors. The protein samples were dissolved in Laemmli buffer and electrophoresed through 4%–15% SDS-PAGE gradient gel followed by transfer to PVDF membrane. The membrane was blocked and treated with primary antibodies against NE Chicken IgY (22), and the rabbit polyclonal antibodies (Cell Signaling Technology) against BAX (catalog 2772), BAD (catalog 9292), BIM (catalog 2819), and anti-BIP (catalog ab21685; Abcam) or β-ACTIN (catalog A5441, clone AC-15, Sigma-Aldrich) followed by washing and subsequent treatment with secondary antibodies tagged with HRP (anti–mouse Ig [catalog 70765, Cell Signaling Technology], anti–rabbit Ig [catalog 70745, Cell Signaling Technology], and goat anti–chicken Ig [catalog ab97135, Abcam]). The blots were developed using a chemiluminescence coupled reaction.

Confocal immunofluorescence microscopy. The sorted promyelocytes were cytospun onto Superfrost Plus microscope slides (Fisher Scientific), airdried and fixed in 4% paraformaldehyde for 30 minutes at 4°C, permeabilized with 0.1% Triton X-100 (catalog T9284, Sigma-Aldrich) for 10 minutes, and blocked with 5% normal goat serum for 30 minutes. The slides were stained with primary antibodies anti-NE and the antibodies (from Abcam) anti-MPO (catalog ab134132, clone EPR4793) or anti-BIP (catalog ab21685) at 4°C overnight. They were washed and then treated with secondary antibodies (from Invitrogen) goat anti–rabbit Alexa Fluor 488 (catalog A11034) or donkey anti–chicken IgY Alexa Fluor 568 (catalog A11041) at 1:500 v/v concentration for 1 hour at room temperature. Cells were washed and mounted using Gold Antifade mounting media (catalog P36935, Invitrogen) containing DAPI. The stained cells were analyzed by

a LSM 710 confocal microscope system (Zeiss) equipped with an inverted microscope (Observer Z1, Zeiss) using a Plan Apochromat ×63 1.4 NA oil immersion lens, and images were processed using Adobe Photoshop v7.

Correction of ELANE exon 3 mutation by CRISPR/Cas9. The human codon-optimized Cas9 plasmids were obtained from Addgene (42230). Two guide RNAs to target 5′ and 3′ of *ELANE* exon 3 were designed using the Zhang lab CRISPR design tool (http://crispr.mit.edu/). The guide RNAs (5′-GAGCCCATAACCTCTCGCGG-3′ and 5′-GAAACGGGAAAATACCCGCCA-3′) were then cloned into the Cas9 vector using a published protocol (56). The donor plasmid with 5′ 0.8 kb and 3′ 1.2 kb homology arms was synthesized by GenScript. *ELANE* CRISPR and donor plasmids were purified using the Endo-Free Maxi Prep Kit (QIAGEN). For genome editing, iPSCs were cultured on 6-well Matrigel-coated dishes in mTeSR1 until confluence (StemCell Technologies Inc.). Cells were dissociated into single cells using accutase (Sigma-Aldrich) and nucleofected using the Amaxa Nucleofector (Lonza) and kit P3 according to manufacturer's instructions with 1 μg CRISPR and 1 μg donor construct. After nucleofection, cells were plated on Matrigel-coated dishes in mTeSR1 media supplemented with 10 μM ROCK inhibitor Y-27632 (Millipore). Cells were allowed to expand for 2–3 weeks after cell sorting to recover. Cells were then dissociated into single cells using accutase, and the GFP^+ (donor-expressing) cells were sorted by FACS. GFP^+ iPSCs were then plated onto Matrigel-coated culture dishes in mTeSR media supplemented with 10 μM ROCK inhibitor Y-27632 for 24 hours. Once iPSC sub-lines were established, iPSCs were transitioned to MEF culture for hematopoietic differentiation.

Statistics. Data are presented as individual data and mean ± SD.

Study approval. This study has been performed following Institutional Review Board approval by the Cincinnati Children's Hospital Medical Center, Cincinnati, Ohio, USA; a written informed consent was received from participants prior to inclusion in the study.

Acknowledgments

This study was supported by the NIH (1R01GM110628), as well as funds from Hoxworth Blood Center (to J.A. Cancelas and C. Lutzko) and Cincinnati Children's Hospital Medical Center (to H.L. Grimes and C. Lutzko). We thank Robin Schroll, Stacy Bush, and Nathaniel Barasa for technical assistance. We thank Cincinnati Children's Research Foundation Mouse, Flow Cytometry, Immunobiology and Cell Processing Cores for their services, supported by the Center of Excellence in Molecular Hematology (P30 DK090971) and the support by an NHLBI Progenitor Cell Consortium Administrative grant that supported the Cincinnati Cell Characterization Core, C4 (5U01 HL099997). We want to thank Margaret O'Leary for editorial assistance.

Address correspondence to: Jose A. Cancelas, Hoxworth Blood Center; 3130 Highland Ave., Cincinnati, Ohio 45267, USA. Phone: 513.558.1324; E-mail: jose.cancelas@cchmc.org. Or to: Carolyn Lutzko, Division of Experimental Hematology and Cancer Biology, Cincinnati Children's Hospital Medical Center, 3333 Burnet Ave., Cincinnati, Ohio 45229, USA. Phone: 513.803.2420; E-mail: carolyn.lutzko@cchmc.org. Or to: H. Leighton Grimes, Division of Immunobiology, Cincinnati Children's Hospital Medical Center, 3333 Burnet Ave., Cincinnati, Ohio 45229, USA. Phone: 513.636.6089; E-mail: lee.grimes@cchmc.org.

1. Berliner N, Horwitz M, Loughran TP Jr. Congenital and acquired neutropenia. *Hematology Am Soc Hematol Educ Program*. 2004;2004:63–79.
2. Horwitz MS, Corey SJ, Grimes HL, Tidwell T. ELANE mutations in cyclic and severe congenital neutropenia: genetics and pathophysiology. *Hematol Oncol Clin North Am*. 2013;27(1):19–41.
3. Donini M, et al. G-CSF treatment of severe congenital neutropenia reverses neutropenia but does not correct the underlying functional deficiency of the neutrophil in defending against microorganisms. *Blood*. 2007;109(11):4716–4723.
4. Rosenberg PS, et al. The incidence of leukemia and mortality from sepsis in patients with severe congenital neutropenia receiving long-term G-CSF therapy. *Blood*. 2006;107(12):4628–4635.
5. Carlsson G, et al. Hematopoietic stem cell transplantation in severe congenital neutropenia. *Pediatr Blood Cancer*. 2011;56(3):444–451.
6. Dale DC, et al. Mutations in the gene encoding neutrophil elastase in congenital and cyclic neutropenia. *Blood*. 2000;96(7):2317–2322.
7. Horwitz M, Benson KF, Person RE, Aprikyan AG, Dale DC. Mutations in ELA2, encoding neutrophil elastase, define a 21-day biological clock in cyclic haematopoiesis. *Nat Genet*. 1999;23(4):433–436.
8. Huntington JA, Read RJ, Carrell RW. Structure of a serpin-protease complex shows inhibition by deformation. *Nature*. 2000;407(6806):923–926.
9. Skokowa J, et al. Interactions among HCLS1, HAX1 and LEF-1 proteins are essential for G-CSF-triggered granulopoiesis. *Nat Med*. 2012;18(10):1550–1559.
10. Skokowa J, et al. NAMPT is essential for the G-CSF-induced myeloid differentiation via a NAD(+)-sirtuin-1-dependent pathway. *Nat Med*. 2009;15(2):151–158.
11. Skokowa J, et al. LEF-1 is crucial for neutrophil granulocytopoiesis and its expression is severely reduced in congenital neutropenia. *Nat Med*. 2006;12(10):1191–1197.
12. Salipante SJ, et al. Contributions to neutropenia from PFAAP5 (N4BP2L2), a novel protein mediating transcriptional repressor cooperation between Gfi1 and neutrophil elastase. *Mol Cell Biol*. 2009;29(16):4394–4405.
13. Newburger PE, et al. Cyclic neutropenia and severe congenital neutropenia in patients with a shared ELANE mutation and paternal haplotype: evidence for phenotype determination by modifying genes. *Pediatr Blood Cancer*. 2010;55(2):314–317.
14. Benson KF, et al. Mutations associated with neutropenia in dogs and humans disrupt intracellular transport of neutrophil elastase. *Nat Genet*. 2003;35(1):90–96.
15. Ron D, Walter P. Signal integration in the endoplasmic reticulum unfolded protein response. *Nat Rev Mol Cell Biol*. 2007;8(7):519–529.
16. Grenda DS, et al. Mutations of the ELA2 gene found in patients with severe congenital neutropenia induce the unfolded protein response and cellular apoptosis. *Blood*. 2007;110(13):4179–4187.
17. Kollner I, et al. Mutations in neutrophil elastase causing congenital neutropenia lead to cytoplasmic protein accumulation and induction of the unfolded protein response. *Blood*. 2006;108(2):493–500.
18. Grenda DS, et al. Mice expressing a neutrophil elastase mutation derived from patients with severe congenital neutropenia have normal granulopoiesis. *Blood*. 2002;100(9):3221–3228.
19. Nanua S, et al. Activation of the unfolded protein response is associated with impaired granulopoiesis in transgenic mice expressing mutant Elane. *Blood*. 2011;117(13):3539–3547.
20. Pomp O, Colman A. Disease modelling using induced pluripotent stem cells: status and prospects. *BioEssays*. 2013;35(3):271–280.
21. Hiramoto T, et al. Wnt3a stimulates maturation of impaired neutrophils developed from severe congenital neutropenia patient-derived pluripotent stem cells. *Proc Natl Acad Sci U S A*. 2013;110(8):3023–3028.
22. Tidwell T, et al. Neutropenia-associated ELANE mutations disrupting translation initiation produce novel neutrophil elastase isoforms. *Blood*. 2014;123(4):562–569.
23. Mills JA, Paluru P, Weiss MJ, Gadue P, French DL. Hematopoietic differentiation of pluripotent stem cells in culture. *Methods Mol Biol*. 2014;1185:181–194.
24. Kattman SJ, et al. Stage-specific optimization

of activin/nodal and BMP signaling promotes cardiac differentiation of mouse and human pluripotent stem cell lines. *Cell Stem Cell*. 2011;8(2):228–240.
25. Pincus SH, Boxer LA, Stossel TP. Chronic neutropenia in childhood. Analysis of 16 cases and a review of the literature. *Am J Med*. 1976;61(6):849–861.
26. L'Esperance P, Brunning R, Good RA. Congenital neutropenia: in vitro growth of colonies mimicking the disease. *Proc Natl Acad Sci U S A*. 1973;70(3):669–672.
27. Takayama S, et al. Evolutionary conservation of function among mammalian, avian, and viral homologs of the Bcl-2 oncoprotein. *DNA Cell Biol*. 1994;13(7):679–692.
28. Hsu PD, et al. DNA targeting specificity of RNA-guided Cas9 nucleases. *Nat Biotechnol*. 2013;31(9):827–832.
29. Horwitz MS, Duan Z, Korkmaz B, Lee HH, Mealiffe ME, Salipante SJ. Neutrophil elastase in cyclic and severe congenital neutropenia. *Blood*. 2007;109(5):1817–1824.
30. Freedman MH, et al. Myelodysplasia syndrome and acute myeloid leukemia in patients with congenital neutropenia receiving G-CSF therapy. *Blood*. 2000;96(2):429–436.
31. Dahl R, et al. Regulation of macrophage and neutrophil cell fates by the PU.1:C/EBPα ratio and granulocyte colony-stimulating factor. *Nat Immunol*. 2003;4(10):1029–1036.
32. Hirai H, et al. C/EBPbeta is required for 'emergency' granulopoiesis. *Nat Immunol*. 2006;7(7):732–739.
33. Skokowa J, Welte K. Defective G-CSFR signaling pathways in congenital neutropenia. *Hematol Oncol Clin North Am*. 2013;27(1):75–88.
34. Borregaard N, Cowland JB. Granules of the human neutrophilic polymorphonuclear leukocyte. *Blood*. 1997;89(10):3503–3521.
35. Filali M, Cheng N, Abbott D, Leontiev V, Engelhardt JF. Wnt-3A/β-catenin signaling induces transcription from the LEF-1 promoter. *J Biol Chem*. 2002;277(36):33398–33410.
36. Gullberg U, Bengtsson N, Bulow E, Garwicz D, Lindmark A, Olsson I. Processing and targeting of granule proteins in human neutrophils. *J Immunol Methods*. 1999;232(1–2):201–210.
37. Gullberg U, Lindmark A, Lindgren G, Persson AM, Nilsson E, Olsson I. Carboxyl-terminal prodomain-deleted human leukocyte elastase and cathepsin G are efficiently targeted to granules and enzymatically activated in the rat basophilic/mast cell line RBL. *J Biol Chem*. 1995;270(21):12912–12918.
38. Massullo P, et al. Aberrant subcellular targeting of the G185R neutrophil elastase mutant associated with severe congenital neutropenia induces premature apoptosis of differentiating promyelocytes. *Blood*. 2005;105(9):3397–3404.
39. Egesten A, Breton-Gorius J, Guichard J, Gullberg U, Olsson I. The heterogeneity of azurophil granules in neutrophil promyelocytes: immunogold localization of myeloperoxidase, cathepsin G, elastase, proteinase 3, and bactericidal/permeability increasing protein. *Blood*. 1994;83(10):2985–2994.
40. Grskovic M, Javaherian A, Strulovici B, Daley GQ. Induced pluripotent stem cells — opportunities for disease modelling and drug discovery. *Nat Rev Drug Discov*. 2011;10(12):915–929.
41. Gunaseeli I, Doss MX, Antzelevitch C, Hescheler J, Sachinidis A. Induced pluripotent stem cells as a model for accelerated patient- and disease-specific drug discovery. *Curr Med Chem*. 2010;17(8):759–766.
42. Deng W. Induced pluripotent stem cells: paths to new medicines. A catalyst for disease modelling, drug discovery and regenerative therapy. *EMBO Rep*. 2010;11(3):161–165.
43. Morishima T, et al. Genetic correction of HAX1 in induced pluripotent stem cells from a patient with severe congenital neutropenia improves defective granulopoiesis. *Haematologica*. 2014;99(1):19–27.
44. Hu P, Han Z, Couvillon AD, Exton JH. Critical role of endogenous Akt/IAPs and MEK1/ERK pathways in counteracting endoplasmic reticulum stress-induced cell death. *J Biol Chem*. 2004;279(47):49420–49429.
45. Murakami Y, Aizu-Yokota E, Sonoda Y, Ohta S, Kasahara T. Suppression of endoplasmic reticulum stress-induced caspase activation and cell death by the overexpression of Bcl-xL or Bcl-2. *J Biochem*. 2007;141(3):401–410.
46. Souza LR, Silva E, Calloway E, Cabrera C, McLemore ML. G-CSF activation of AKT is not sufficient to prolong neutrophil survival. *J Leukoc Biol*. 2013;93(6):883–893.
47. Iwata A, et al. Extracellular administration of BCL2 protein reduces apoptosis and improves survival in a murine model of sepsis. *PLoS One*. 2011;6(2):e14729.
48. Skokowa J, Welte K. Dysregulation of myeloid-specific transcription factors in congenital neutropenia. *Ann N Y Acad Sci*. 2009;1176:94–100.
49. Feng L, Zhu W, Huang C, Li Y. Direct interaction of ONO-5046 with human neutrophil elastase through (1)H NMR and molecular docking. *Int J Biol Macromol*. 2012;51(3):196–200.
50. Kunisato A, Wakatsuki M, Shinba H, Ota T, Ishida I, Nagao K. Direct generation of induced pluripotent stem cells from human nonmobilized blood. *Stem Cells Dev*. 2011;20(1):159–168.
51. Kim YE, Hipp MS, Bracher A, Hayer-Hartl M, Hartl FU. Molecular chaperone functions in protein folding and proteostasis. *Annu Rev Biochem*. 2013;82:323–355.
52. Rajan RS, Tsumoto K, Tokunaga M, Tokunaga H, Kita Y, Arakawa T. Chemical and pharmacological chaperones: application for recombinant protein production and protein folding diseases. *Curr Med Chem*. 2011;18(1):1–15.
53. Warlich E, et al. Lentiviral vector design and imaging approaches to visualize the early stages of cellular reprogramming. *Mol Ther*. 2011;19(4):782–789.
54. Lucas SD, Costa E, Guedes RC, Moreira R. Targeting COPD: advances on low-molecular-weight inhibitors of human neutrophil elastase. *Med Res Rev*. 2013;33(suppl 1):E73–E101.
55. Kawabata K, Suzuki M, Sugitani M, Imaki K, Toda M, Miyamoto T. ONO-5046, a novel inhibitor of human neutrophil elastase. *Biochem Biophys Res Comm*. 1991;177(2):814–820.
56. Ran FA, Hsu PD, Wright J, Agarwala V, Scott DA, Zhang F. Genome engineering using the CRISPR-Cas9 system. *Nat Protoc*. 2013;8(11):2281–2308.